

Formation and past evolution of the showers of 96P/Machholz complex



Abedin Abedin^{a,b,*}, Paul Wiegert^{a,b}, Diego Janches^c, Petr Pokorný^{c,d}, Peter Brown^{a,b}, Jose Luis Hormaechea^e

^a Department of Physics and Astronomy, The University of Western Ontario, London, N6A 3K7, Canada

^b Centre for Planetary Science and Exploration (CPSX), The University of Western Ontario, London, N6A 3K7, Canada

^c Space Weather Laboratory, GSFC/NASA, 20771, Greenbelt MD

^d Department of Physics, The Catholic University of America, Washington, DC 20064, USA

^e Facultad de Cs. Astronomicas y Geofisicas, UNLP, y CONICET, Estacion Astronomica Rio Grande, Tierra del Fuego, Argentina

ARTICLE INFO

Article history:

Received 26 October 2016

Revised 11 June 2017

Accepted 21 July 2017

Available online 25 July 2017

ABSTRACT

In this work we model the dynamical evolution of meteoroid streams of comet 96P/Machholz, and the largest member of the Marsden sunskirters, comet P/1999 J6. We simultaneously fit the characteristics of eight meteor showers which have been proposed to be linked to the complex, using observations from a range of techniques - visual, video, TV and radar. The aim is to obtain a self-consistent scenario of past capture of a large comet into a short-period orbit, and its subsequent fragmentation history. Moreover, we also aim to constrain the dominant parent of these showers.

The fit of our simulated shower characteristics to observations is consistent with the scenario of a capture of a proto-comet 96P/Machholz by Jupiter circa 20000 BCE, and a subsequent major breakup around 100–950 CE which resulted in the formation of the Marsden group of comets. We find that the Marsden group of comets are not the immediate parents of the daytime Arietids and Northern and Southern δ -Aquiids, as previously suggested. In fact, the hypothesis that the Northern δ -Aquiids are related to the Marsden group of comets is not supported by this study.

The bulk of the observational characteristics of all eight showers can be explained by meteoroid ejection primarily from comet 96P/Machholz between 10000 BCE and 20000 BCE. Assuming the Marsden group of comets originated between 100 CE–950 CE, we conclude that sunskirting comets contribute mainly to the meteoroid stream near the time of the peak of the daytime Arietids, Southern δ -Aquiids, κ -Velids. Finally, we find that the meteor showers identified by Babadzhanyan and Oubrov (1992) as the α -Cetids, the Ursids and Carinids correspond to the daytime λ -Taurids, the November ι -Draconids or December α -Draconids and the θ -Carinids.

© 2017 Published by Elsevier Inc.

1. Introduction

This work builds on a series of studies aiming to investigate the origin and past evolution of the meteoroid complex related to comet 96P/Machholz (96P hereafter). In a previous work, we investigated the formation mechanism and the age of the Quadrantid meteoroid stream (Abedin et al., 2015) and more recently the origin of the daytime Arietids meteor shower (Abedin et al., 2017). Our main goal is to develop a self-consistent scenario of the hierarchical fragmentation and subsequent evolution of the 96P complex, using detailed observational characteristics of the associated Machholz shower complex.

Comet 96P is unusual among the short-period comets. It has an extremely low perihelion distance, grazing the Sun at a distance of 0.123 AU or roughly $27R_{\odot}$, and has been associated with up to eight meteor showers, several other comets and at least one object of asteroid appearance. In particular, it is thought that 96P shares a genetic relationship with the Marsden and Kracht group of sunskirting comets and the Kreutz sungrazers (e.g., Sekanina and Chodas, 2005; Jenniskens, 2006). This ensemble of interplanetary bodies is referred to as the Machholz interplanetary complex and is believed to have originated from a single split of a larger progenitor prior to 950 CE (Sekanina and Chodas, 2005). Despite the association of 96P with the aforementioned bodies, some of their present orbital elements differ noticeably, owing to differential planetary perturbations (mainly due to Jupiter). Presently, the Marsden sunskirters approach the Sun within 8.8–11.2 R_{\odot} (Sekanina and Chodas, 2005), and have mean orbital inclination

* Corresponding author.

E-mail address: aabedin@uwo.ca (A. Abedin).

of $\approx 26^\circ$, whereas the Kracht group of comets have perihelia in the range $6.7 - 11.6R_\odot$ and inclination of $\approx 13^\circ$. For comparison, the present inclination of 96P is $i \approx 58^\circ$ and perihelion distance of 0.123 AU ($\approx 27R_\odot$). Furthermore, 96P is interesting among other comets as it has anomalous molecular abundances (e.g., A'Hearn et al., 1995; Schleicher, 2008), being relatively depleted in CN, C_2 , C_3 compared to the OH abundance. That indicates that 96P has either formed in a region of the early Solar system with unusual conditions or is interstellar in origin.

Comet 96P was mentioned for the first time in the context of meteor astronomy by McIntosh (1990). The author noted the similar orbital evolution of 96P and the Quadrantid meteoroid stream, though their evolutionary cycles were offset by 4000 years. That led McIntosh (1990) to suggest a sibling rather than child-parent relationship.

Numerical simulations of the long-term evolution of the orbit of 96P were performed by Babadzhanov and Obruov (1992). They were the first to suggest that within one circulation cycle of the longitude of the ascending node Ω and the argument of perihelion ω (≈ 8200 years), the comet may give rise to eight different meteor showers. The Earth intersects four of these showers at their descending nodes and four at their ascending nodes. The authors identified these showers as the Quadrantids, daytime Arietids, Southern and Northern δ -Aquariids, Ursids, κ -Velids, Carinids and the α -Cetids. This work was extended by Babadzhanov et al. (2008) who considered instead asteroid 2003 EH₁ as the parent (a known member of the 96P complex, see Section 1.1.1), where they obtained similar results for the first four showers, but the four last showers were linked to the α -Draconids, Puppis-Velids, Carinids and α -Piscids respectively. In short, the first four showers are well known and constrained. The existence of the other showers has remained uncertain, partly due to the lack of systematic meteor surveys from the Southern hemisphere.

Jones and Jones (1993) argued that if comet 96P had been captured by close approach with Jupiter about 2200 years ago, there has been sufficient time for the comet to produce most of the observed characteristics of the Quadrantids, the daytime Arietids and Southern δ -Aquariids.

Recent work carried out by Neslušan et al. (2013b) investigated potential streams related to 96P, assuming an initial meteoroid ejection time 4000 years ago. They concluded that 96P may indeed produce eight different showers, though they were skeptical about the detectability of all of them. Instead, they argued that due to the proximity of four of the intersection points with the Earth's orbit, only six showers are expected to be identified. Although the authors recognized the ~ 8200 year circulation cycle of the longitude of the ascending node and the argument of perihelion of 96P's orbit, they considered only half of that period in their investigation. Moreover, the authors did not compare the characteristics of the modeled meteoroid streams in detail with available observations.

Several recent works have suggested that the Marsden group of comets are the immediate parents of the daytime Arietids and the Northern and Southern δ -Aquariids (Ohtsuka et al., 2003; Sekanina and Chodas, 2005; Jenniskens, 2006; Jenniskens et al., 2012). Ohtsuka et al. (2003) noted the similarity in the orbital evolution of 96P, the Marsden and Kracht group of sunskirting comets and the daytime Arietids, assuming their evolutionary cycles were shifted by a few hundred years. The authors suggested that the Arietids are related to the Marsden group but hinted that all bodies may be genetically related. Sekanina and Chodas (2005) performed numerical simulations to investigate the origin of the Marsden and Kracht group of comets. Based on the tendency of these comets to arrive at perihelion in pairs, the authors developed a detailed model and suggested that the sunskirting group of comets, along with the Arietids and southern δ -Aquariids, originated from a single comet

break up prior to 950 CE. However, these authors and earlier works have not attempted to constrain formation models of the 96P complex using detailed observations of the associated meteor showers.

1.1. 96P/Machholz complex showers

Some of the individual showers belonging to 96P complex have already been studied by several authors, including our series of studies. Below, we provide a brief summary of each shower, listed according their strengths:

1.1.1. The Quadrantids

The Quadrantids are unusual, being among the strongest of the annual showers with an extremely compact central portion, with a Full Width of Half Maximum (FWHM) of only ≈ 17 h, encountered every year between January 3–4. The short duration alone is a strong evidence that the core of the stream is young.

Due to the presently large difference in the longitude of the ascending nodes of the stream and 96P/Machholz, the comet was not recognized as the immediate parent of the stream. Comet 1491 I was suggested by Hasegawa (1979) and followed up by others (Hasegawa, 1979; Williams and Collander-Brown, 1998; Williams et al., 2004; Jopek and Williams, 2013); however the relatively poor orbit that could derived from ancient Chinese, Japanese and Korean records (Kronk, 1999) makes a clear link difficult. Numerous other cometary parents have been considered (see Williams et al., 2004 for a review) but were found wanting. Jenniskens et al. (1997) suggested that the parent may be an asteroid-like object, hidden in a high inclination orbit. With the discovery of asteroid 2003 EH₁, Jenniskens (2004) noted a striking similarity with the orbit of the Quadrantids and suggested a child-parent relationship. Wiegert and Brown (2005) performed a nodal regression analysis of the orbits of 2003 EH₁ and the Quadrantids, arguing that the core of the stream is only 200 years old. Williams et al. (2004) performed a similar study which concluded the stream was young, as 2003 EH₁ and the Quadrantids were on similar orbits 500 years ago.

However, recent radar observations of the Quadrantids revealed that there is an older component of the stream, lasting from mid-November to mid-January (Brown et al., 2010). Using seven high-precision photographic Quadrantids, augmented with radar observations by the *Canadian Meteor Orbit Radar* (CMOR) we demonstrated, from back-integrations of eight high precision photographic Quadrantid and five high-precision radar Quadrantids, that the core of the stream is related to asteroid 2003 EH₁ and most likely formed circa 1800 CE (Abedin et al., 2015). This study also found that the older component is associated with comet 96P and is several millenia old. For a more detailed review of past works on the Quadrantids, the reader is referred to Jenniskens (2006), Neslušan et al. (2013b) and Abedin et al. (2015).

1.1.2. The daytime Arietids

This shower is observed annually between mid-May and late June with a broad plateau of peak activity near solar longitude $\lambda_\odot = 80.5^\circ$ (Bruzzone et al., 2015). The shower characteristics have mostly been constrained by radar observations, owing to the proximity of the radiant position to the Sun, with some recent optical observations. Recently, we addressed the question as to the association of the stream with the Marsden group of comets or comet 96P (as discussed above). We performed detailed numerical simulations of meteoroids, ejected from 96P and the most notable member of the Marsden group of comets - P/1999 J6. The resulting streams from both comets were analyzed with respect to which could reproduce the main characteristics of the daytime Arietids. As observational constraints for the shower, we used data from the

12 year radar survey of the daytime Arietids by CMOR (Bruzzone et al., 2015), along with 14 TV observations by SonotaCo (2009) and 31 video events recorded by the Cameras for All-sky Meteor Surveillance (CAMS) (Jenniskens et al., 2016). Our simulations indicated that the Marsden group of comets can not alone reproduce the observed characteristics of the shower and thus can not be the sole parents of the stream. Instead, we conclude that the broader activity of the daytime Arietids is associated with comet 96P and has an age of ~ 12000 years, though we demonstrated that the Marsden group of comets may contribute to the peak of the shower. An outstanding question for this shower relates to the difference in the orbital elements of optical and radar sized particles, a discrepancy previously noted by Jenniskens et al. (2012). Radar surveys measure systematically lower meteoroid geocentric speeds, and thus lower orbital semi-major axes, as compared to those obtained by optical surveys. Jenniskens et al. (2012) attributed these differences to insufficient correction for deceleration of radar sized (a few hundreds of microns) meteoroids in the Earth's atmosphere. These are normally subject to a greater atmospheric drag than larger meteoroids. These differences, if they are real, may imply that the daytime Arietids are older than a few tens of millenia (assuming the difference in the orbital elements is due to Poynting-Robertson drag). The observed discrepancy however, remains unresolved.

1.1.3. Southern and Northern δ -Aquiriids

The Southern δ -Aquiriids are observed every year between late May to early July with peak activity at solar longitude $\lambda_{\odot} = 126^{\circ}$ (Brown et al., 2010). Though much weaker, the northern branch is active between late July to late August with maximum activity occurring at $\lambda_{\odot} = 139^{\circ}$. Although the showers stand well above the sporadic background and have been well measured, their origin has received less attention and is mostly limited to the works by Babadzhanov and Oubrov (1992), Sekanina and Chodas (2005), Jenniskens (2006) and Babadzhanov et al. (2008) and Neslušan et al. (2013b).

1.1.4. κ -Velids, α -Cetids, Carinids and Ursids

The predicted κ -Velids have recently been established as an annual shower (Pokorný et al., 2017), based on systematic radar observations by the Southern Argentina Agile Meteor Radar (SAAMER) (Janches et al., 2013; 2015) and we consider this linkage secure.

The remaining three we will discuss in more detail in this paper, but we note that there is no obvious shower listed in the IAU Meteor Data Center (IAU MDC) (<http://www.ta3.sk/IAUC22DB/MDC2007/>), corresponding to the radiant, speed and timing characteristics predicted by Babadzhanov and Oubrov (1992) for α -Cetids, though there are 19 different showers that are listed as Cetids. The Southern Daytime ω -Cetids may correspond to this shower in Babadzhanov et al. (2008) where they identify it as the α -Piscids. Likewise, there are 4 different showers listed as Carinids, though only θ -Carinids have been well measured (Pokorný et al., 2017). Finally, the association of the Ursids with 96P is questionable, as the stream has already been confirmed to be related to comet 8P/Tuttle (e.g., Jenniskens, 2006), which indicates that the stream had been either misidentified by Babadzhanov and Oubrov (1992) or it overlaps with another nearby stronger meteor shower and hence can not be detected as individual, as previously suggested by Neslušan et al. (2013b).

In this work, we aim to obtain a broader picture of the origin and past evolution of the complex of interplanetary bodies, associated with comet 96P. We approach that problem by simultaneously fitting the observed shower characteristics and attempt to answer the following questions:

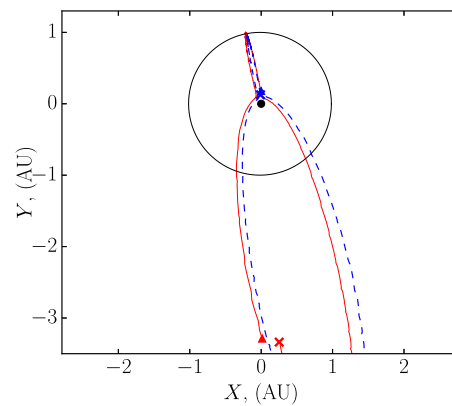


Fig. 1. Backwards time evolution of the ascending (blue dashed line) and descending (red solid line) nodes of the orbit of comet 96P/Machholz for one Kozai circulation cycle (~ 8200 years) of longitude of the ascending node (Ω) and argument of perihelion (ω). The “x” symbols indicate the starting position of the cycle (present) and the triangle denotes the end position. (For interpretation of the references to color in this figure legend, the reader is referred to the web version of this article.)

1. What is the dominant parent of the 96P meteoroid complex, comet 96P/Machholz or the Marsden group of comets?
2. What is the age and likely parent (comet 96P/Machholz or the Marsden group of comets) of the Southern and Northern δ -Aquiriids and the recently established κ -Velids and θ -Carinids?
3. Do the Carinids, α -Cetids and Ursids exist or they have been misidentified? If they exist, what is their likely age and parent?
4. Can we obtain a self-consistent scenario as to the epoch when comet 96P was captured into a short period orbit and its past fragmentation history?

2. Observations

In this section we present the observational characteristics of the showers that we study and also provide some observational constraints on the parent bodies considered in this work.

Babadzhanov and Oubrov (1992) were the first to note that comet 96P may intersect the Earth's orbit at eight different locations, during one Kozai cycle (≈ 8200 years) of its longitude of ascending node. As a result, it could produce 8 meteor showers at Earth. Fig. 1 shows the intersection points of the descending and ascending nodes with the Earth's orbit, after one full Kozai cycle. Some of these showers are well known - The Quadrantids, daytime Arietids, Southern and Northern δ -Aquiriids and κ -Velids. Their observational characteristics have been constrained by both radar and optical meteor surveys. However, the identification of some of the showers, which Babadzhanov and Oubrov (1992) have named the Carinids, α -Cetids and Ursids are uncertain. As noted in the previous section, there are no showers in the IAU MDC which match the characteristics of the Carinids and α -Cetids as given by Babadzhanov and Oubrov (1992). The shower designated as Ursids by Babadzhanov and Oubrov (1992) is not well documented in the literature and should not be mistaken with the 00015 (URS) Ursids in the IAU MDC, which is a different shower, unambiguously associated with 8P/Tuttle (Jenniskens et al., 2002). Therefore, as part of this work, we aim to examine the validity of these “misidentified” showers by fitting our simulated shower characteristics to the observations of the well constrained showers (QUA, ARI, SDA, NDA and KVE) and then performing a search for the predicted showers in radar and optical databases.

For the shower data required in this study, such as shower duration, orbits and radiants, we use the orbits measured by the Canadian Meteor Orbit Radar (CMOR) (Brown et al., 2010) and by

the Southern Argentina Agile Meteor Radar (SAAMER) (Janches et al., 2013; 2015). The CMOR dataset includes 1.5×10^7 orbits obtained between 2002 and 2015, while the SAAMER dataset includes 10^6 orbits obtained between 2012 and 2015. For this work we compile these datasets into a representative composite year.

We took the simulation results which predict where shower radiants are expected, together with the expected speed and timing and performed a 3D wavelet search following the methodology described in Brown et al. (2010) and updated in Pokorný et al. (2017). For all predicted radiants we extended our search $\pm 10^\circ$ relative to the predicted radiant and ten degrees of solar longitude before and after the expected activity dates based on the simulations. Finally, we searched over a window of $\pm 10 \text{ km s}^{-1}$ from the predicted speeds for each shower. Our wavelet transforms were computed in steps of 0.2° (providing a lower bound to our radiant precision) and in steps of 0.5% in speed. We used fixed wavelet probe sizes of 4° in angular coordinates and 12% probe size in speed, based on results from Campbell-Brown and Brown (2015) and Pokorný et al. (2017). From these wavelet computations we identified local maxima, which we define as being excursions in the wavelet coefficient of 3σ above the median background based on the year of data outside the shower window, that fell in our analysis windows. Based on the variance in daily radiant location and speed, we estimated our uncertainties to be 1° in radiant position and 5% in speed - these uncertainties are used for all subsequent estimates of error in daily mean shower orbital elements. Finally, we automatically link shower maxima together if individual maxima occur within 2° (or less) in solar longitude, have radiants less than two degrees apart in sun-centered radiant coordinates and are less than 10% different in speed. These search results turned out to be very clean: there was only one possible maxima each day associated with the 96P predicted showers. We also attempted to link each maxima point with pre-existing showers listed in the IAU MDC, assuming common radiants were within 3° in angular coordinates and 10% in speed.

As a result of the search and our stream modelling, we have identified three observed showers as likely part of the 96P complex and roughly similar to the original predictions by Babadzhanov and Obruchov (1992). These are the “December α -Draconids” (IAU #00334, DAD) that partially overlaps with the “November ι -Draconids” (IAU #00392, NID), the “daytime λ -Taurids” (IAU #00325, DLT), “ θ -Carinids” (IAU #00785, TCD). The DADs and the NIDs belong to the northern toroidal source and are the Ursids counterpart identified by Babadzhanov and Obruchov (1992). The DLTs are the southern branch of the daytime Arietids and are likely the shower named α -Cetids by Babadzhanov and Obruchov (1992). Finally, the TCD belong to the southern toroidal source and have only recently been established as a separate meteor shower (Pokorný et al., 2017). Analyzing the observed CMOR shower characteristics of the DAD and NID, we found that the latter two showers are weak and partially overlap in time, which renders their identification as separate showers difficult. We note that these two showers have been identified as separate events in the IAU MDC. Furthermore, towards the end of the activity of the DAD ($\lambda_{\odot \text{end}} = 271.5^\circ$), there is significant background activity that overlaps with the onset of the Quadrantids. In fact, Brown et al. (2010) argued that Quadrantids show a low background activity that lasts about two months. In light of our simulations and more sensitive shower search, we suggest that this extended activity is not in fact one long individual shower, but instead likely three similar showers of the 96P complex, sharing similar radiant and orbital characteristics but slightly offset in nodal times.

The observational characteristics of all of these showers are summarized in Table 1, as derived from radar (CMOR and SAAMER) and optical (CAMS) surveys. Generally, radar and optical meteor detections sample different meteoroid sizes, with the former being

capable of detecting particles of a few hundreds of microns in size, whereas the optical techniques detect larger meteoroids (millimeter and larger). Thus, combining radar and optical observations enables us to fit our stream modelling to observed shower characteristics, equivalent to a few hundred micrometers and millimeter size meteoroids, as well as to investigate the past evolution of meteoroids of different sizes.

In Section 4 we fit the parameters listed in Table 1 directly to our simulations. By simultaneous match of all eight showers, our goal is to obtain age estimates of the showers and put into perspective the origin of the 96P complex.

2.1. Test parent bodies

In this work, we consider two parent bodies for testing a child-parent relationship with the observed meteor showers. These bodies are the comet 96P/Machholz and the most prominent member of the Marsden group of comets, P/1999 J6. The latter was chosen as it has the best constrained orbit among other group members. It would be impractical to simulate the meteoroid streams originating from each individual member of the Marsden group of sunskirters.

Comet P/1999 J6 was first observed by the coronagraph onboard of the *Solar and Heliospheric Observatory* (SOHO) and according to NASA's JPL Horizon database has been classified as a Jupiter-Family Comet (JFC) (<http://ssd.jpl.nasa.gov/sbdb.cgi>), despite its low Tisserand parameter with respect to Jupiter ($T_j = 1.942$), a value more typical for Halley type comets. Generally, JFCs have typical Tisserand parameters with respect to Jupiter of $2 < T_j < 3$. The present period of the comet is $P = 5.46$ years and based on 267 observations it has the orbital elements listed in Table 2. Presently, P/1999 J6 approaches the Sun within $q \approx 0.049$ AU or roughly $10R_\odot$.

Comet 96P/Machholz was discovered on May 12, 1986 and has also been classified as a JFC (<http://ssd.jpl.nasa.gov/sbdb.cgi>). According to the NASA's JPL Horizon database it has an orbital period of $P \sim 5.3$ years, with a Tisserand parameter with respect to Jupiter of $T_j = 1.942$. Similar to P/1999 J6, this value is low and more typical of Halley type comets. The present orbital elements of 96P are listed in Table 2. Presently, the perihelion distance of 96P is $q \approx 0.124$ AU or roughly $25R_\odot$.

The present orbits of the two hypothetical parents, comets 96P and P/1999 J6, are presented in Fig. 2. It is evident that the two orbits are strikingly similar, indicating a possible genetic relationship. Currently, the ascending node of the orbit of 96P is located near the Sun, whereas the descending node is between the orbits of Mars and Jupiter. In contrast, while the ascending node of P/1999 J6 is also close to the Sun, the descending node is close to the Earth's orbit and most likely supplies “young” meteoroids that are presently encountered by the Earth.

3. Numerical simulations

3.1. Solar system model and numerical integrator

In our simulations, we model the Solar system as comprising the Sun and all planets. Effectively, the parents and their synthetic meteoroid streams will move under the gravitational attraction from the Sun, where the planets will act as perturbing forces on their Keplerian motion. We account for the mutual interaction between the planets, while the parent clones and individual meteoroids are considered as test particles. In addition to gravitational effects, the meteoroids will be also subjected to non-gravitational forces such as the solar radiation pressure force (e.g., Burns et al., 1979; Poynting-Robertson (PR) drag (e.g., Burns et al., 1979; Klačka, 2004; Klačka and Kocifaj, 2008). The solar radiation pressure affects the dynamics of micron and millimeter sized particles

Table 1

Geocentric characteristics of the meteor showers, possibly associated with the Machholz complex at their time of maximum activity. The columns denote: 1. The solar longitude of the start time of the activity profile, 2. The time of maximum activity, 3. The end time of the activity, 4. Sun-centered ecliptic longitude of the radiant, 5. Ecliptic latitude of the radiant, 6. Geocentric speed, 7. Geocentric equatorial right-ascension of radiant position in J2000.0. 8. Geocentric equatorial declination of the radiant in J2000.0. The remaining columns list the orbital elements at maximum activity. The superscript (a) indicates data obtained by CMOR, (b) corresponds to CAMS data, (c) observations derived by SAAMER and (d) corresponds to visual observations by IMO.

Shower	$\lambda_{\odot start}$ (deg)	$\lambda_{\odot max}$ (deg)	$\lambda_{\odot end}$ (deg)	$\lambda - \lambda_{\odot}$ (deg)	b (deg)	V_g (km s ⁻¹)	α_g (deg)	δ_g (deg)	a (AU)	q (AU)	e	i (deg)	ω (deg)
QUA ^a	267.5	283.0	291.0	273.0	64.0	41.7	231.0	48.5	2.77	0.977	0.648	71.7	169.5
QUA ^b	270.0	283.0	296.4	277.5	63.7	40.7	230.2	49.5	2.82	0.979	0.657	71.2	171.4
QUA ^d	275.2	283.0	288.6	–	–	–	–	–	–	–	–	–	–
ARI ^a	62.0	80.5	95.0	348.3	7.4	39.1	44.9	25.5	1.71	0.074	0.957	30.6	26.4
ARI ^b	73.0	77.0	89.4	331.6	7.3	41.1	43.9	24.4	2.67	0.078	0.974	27.7	28.7
SDA ^a	114.5	123.5	163.5	210.9	–7.2	41.3	338.8	–16.7	2.23	0.058	0.974	31.5	155.7
SDA ^b	117.9	128.0	145.9	208.8	–7.2	41.3	341.3	–15.7	2.59	0.069	0.975	29.0	152.9
SDA ^d	109.8	124.5	144.4	–	–	–	–	–	–	–	–	–	–
NDA ^a	126	139	156	208.8	7.8	37.3	345.2	2.6	1.70	0.096	0.944	24.8	329.9
NDA ^b	120.9	141.0	207.5	208.4	6.8	38.4	347.6	2.1	1.97	0.090	0.955	22.3	330.7
NDA ^d	113.4	149.0	151.1	–	–	–	–	–	–	–	–	–	–
DLT ^a	71	86	98	331.2	–8.6	35.6	52.5	10.1	1.49	0.109	0.927	23.5	211.1
NID ^a	221.0	241.0	264.0	265.1	61.6	43.0	196.1	65.3	2.44	0.984	0.598	73.7	188.1
NID ^b	239.3	242.0	267.9	260.9	63.2	42.0	196.5	68.3	3.62	0.973	0.734	72.9	194.7
DAD ^b	248.8	256.0	262.6	272.0	62.8	40.8	210.8	58.6	2.48	0.983	0.603	71.8	177.4
TCD ^c	274.0	276.0	280.0	282.3	–60.3	41.7	156.8	–59.2	2.38	0.966	0.595	74.5	342.2
KVE ^c	272.0	276.0	286.0	257.8	–60.5	40.5	141.1	–51.0	2.08	0.965	0.560	72.9	19.1

Table 2

Orbital elements of comet P/1999 J6 and comet 96P/Machholz used in this study, taken from the NASA's JPL Horizon System. See the text for more details.

Name	a (AU)	e	i (deg)	Ω (deg)	ω (deg)
P/1999 J6	3.100499137	0.984177313	26.613141	81.613781	21.976803
±	0.000027986	0.000015813	0.020234	0.072701	0.080133
96P	3.033939724939583	0.95921182874981	58.312214235	94.323236311	14.757748401
±	0.000000024505	0.00000046985	0.000044922	0.000011819	0.000020956

and manifests itself as weakening of the solar gravitational attraction force F_G . Usually, the radiation force is considered via the standard β -parameter and is given by Burns et al. (1979) as:

$$\beta = \frac{F_R}{F_G} = 5.7 \times 10^{-4} \frac{Q_{pr}}{\rho s}, \quad (1)$$

where ρ is the meteoroid's bulk density in kg m⁻³, s is the radius of the meteoroids in meters and Q_{pr} is the light scattering efficiency, considered to be unity in our simulations. PR drag decreases a particle's semi-major axis and eccentricity due to anisotropic emission of the absorbed solar radiation in the reference frame of the Sun, and causes meteoroids to slowly spiral towards the Sun. In this work we do not account for the Lorentz force and solar wind drag as they are ~ 1000 times smaller than the solar radiation pressure (e.g., Leinert and Grun, 1990) for 100 μ m particles (the smallest meteoroids considered here) and their influence decreases for larger meteoroids.

The radiation forces are virtually zero for the considered parent bodies. The only significant non-gravitational force on comet nuclei is the "rocket" like acceleration induced by the sublimation of the cometary volatiles, which causes the trajectory of a comet to deviate from pure gravitational motion. However, we do not model these forces here, due to their stochastic nature over the time scales considered in this work. Thus, the parent bodies will be subject to gravitational force only. Furthermore, the orbital evolution of both parents 96P and P/1999 J6 are in state of Kozai-type oscillation (Section 3.3.1). That leads episodically to decreases of their perihelia to distances of 0.025 AU or roughly $5R_{\odot}$. For this reason, despite the fact that a body would generally spend a very

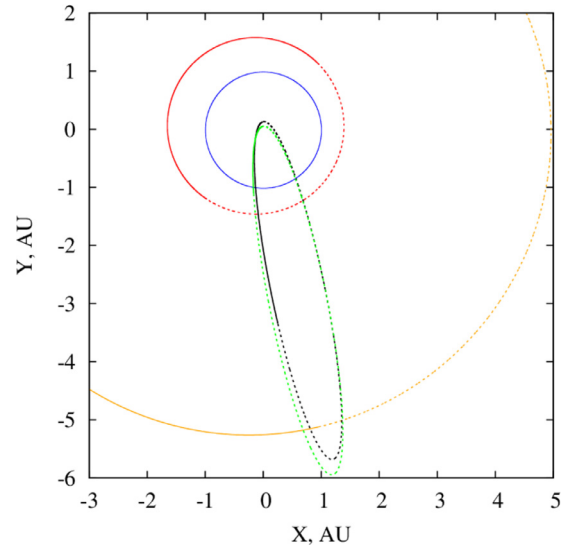


Fig. 2. The orbits of comet 96P/Machholz (black line) and comet P/1999 J6 (green line) viewed from above the ecliptic plane. The solid lines indicate the portion of the orbits above the ecliptic whereas the dotted lines denote the portions below the ecliptic. (For interpretation of the references to color in this figure legend, the reader is referred to the web version of this article.)

short time near perihelion, we also include general relativistic effects (post-Newtonian approximation).

The equations of motion of all bodies (planets, parent bodies and meteoroids) are integrated using the symplectic method

of Wisdom and Holman (1991), with close approaches handled with the Chambers' hybrid symplectic scheme (Chambers, 1999). During the backward integrations of the orbits of 96P and P/1999 J6, we take snapshots of the state vectors of the clones and the planets every year. These state vectors will be used as the basis for meteoroid ejections at any instant of time from suitably selected clones for both parents.

3.2. Meteoroid ejection

The meteoroids are modeled as spherical particles of density $\rho_m = 2500 \text{ kg m}^{-3}$ with radii ranging from $s = 100 \text{ }\mu\text{m}$ (a size appropriate for radar meteors (e.g., Weryk and Brown, 2013)) to $s = 1 \text{ mm}$ (a typical value for optical or visual meteors). They are sampled from a uniform distribution of the logarithm of their radii. Although, this is not a realistic size distribution, we aim to sample a wide size range of meteoroid sizes in order to investigate the resulting shower for radar and optical size meteors. Later, we apply weighting to the number of meteoroids as a function of their size (Sections 3.4.6 and 3.4.5).

The meteoroids are ejected as a result of cometary outgassing, where the ejection speed is modeled according to Brown and Jones (1998) and is given as:

$$V_{\text{ej}} = 10.2r^{-1.038} \rho^{-1/3} R_c^{1/2} m^{-1/6} \text{ (m s}^{-1}\text{)} \quad (2)$$

where r is the heliocentric distance (AU), ρ is the bulk density of the meteoroid (g cm^{-3}), R_c is the radius of the comet nucleus (km) and m is the mass of the meteoroid (grams). The meteoroids are ejected isotropically on the sunlit hemisphere independently of the angle to the Sun. The dust production rate is assumed to be uniform in true anomaly of the parent in the simulation. Thus, in order to calculate the ejection speeds, we also need to know the parents' physical size.

Recent studies of the nucleus brightness suggest a radius for 96P between $R = 2 - 2.5 \text{ km}$ (e.g., Green et al., 1990; Sekanina, 1990; Licandro et al., 2000) and more recently $R = 3.2 \text{ km}$ (Lamy et al., 2004). We model comet 96P as a spherical nucleus of a mean radius $R = 2.5 \text{ km}$ and bulk density of $\rho = 700 \text{ kg m}^{-3}$. Despite P/1999J6 being the largest fragment of the Marsden group of comets, and that it has survived at least several perihelion returns, Sekanina and Chodas (2005) estimated that the nucleus of the comet is not greater than 45m. However, Lamy et al. (2013) questioned these estimates based on more recent analysis of light-curves of sunskirting comets and concluded that the size of the largest fragments must be at least a few hundreds of meters. Following the results of that recent work, we assume a radius for P/1999J6 of $R = 0.25 \text{ km}$ and bulk density of $\rho = 700 \text{ kg m}^{-3}$.

For example, the mass of a meteoroid at the lower size range ($s = 100 \text{ }\mu\text{m}$), considered in our simulations, would have a value of $m \approx 10^{-6}$ grams. The magnitude of the ejection speed for such a meteoroid, released from the nucleus of 96P/Machholz at a heliocentric distance of 1 AU would be $V_{\text{ej}} \approx 160 \text{ m s}^{-1}$, whereas meteoroid of radius $s = 1 \text{ mm}$ would have a terminal speed of $V_{\text{ej}} \approx 50 \text{ m s}^{-1}$. We note, however, that there is no reliable way to know what the actual size of the comet was about 20,000 years in the past. If the nucleus of 96P was as twice as big, 20,000 years ago as its present size, the above values of the ejection speeds will translate to $V_{\text{ej}} \approx 226 \text{ m s}^{-1}$ for a radar size meteoroid and $V_{\text{ej}} \approx 70.5 \text{ m s}^{-1}$ for a particle of radius $s = 1 \text{ mm}$. However, we do not expect that the uncertainty introduced by the lack of knowledge on the original parent size 20,000 years into the past to be significant. This is because the meteoroids are expected to have initial orbits similar to that of the parents, and the difference in ejection speeds are much lower than the orbital speeds of the parents. Thus the effect on the difference in ejection speeds due to differences in the original parent size will be significantly smaller

than the errors in the 'true' orbital evolution of the parent over a 20,000 year period.

P/1999 J6 is significantly smaller and fainter than 96P, so it is not unreasonable to expect that it will have less dust production compared to 96P. However, here we will initially assume dust production rate similar to 96P merely because we need to eject a relatively large number of particles from both parents so we have a good particle number statistics. This seems a reasonable assumption, since our goal is to test the streams to see which parent body will produce a better match to the observed width of the activity profiles, which is to a first order a proxy as to the age of the shower. The amount of dust production is not expected to affect the width of the profiles but only the relative number of particles in each bin of the solar longitude. The size of the cross-section of a stream, and thus the width of the activity profile, will depend on the differential planetary perturbations and non-gravitational forces over time.

3.2.1. Selecting "clones" for backward integrations

The first step in meteoroid stream modelling is to integrate the orbit of a hypothetical parent back in time to an epoch of interest that will be used for meteoroid ejection and forward integrations. Despite the good quality of contemporary small Solar system body observations, their "true" orbits are not exactly known but instead come with a confidence region. Therefore we sample the uncertainty region of the phase space of their orbital elements, aiming to consider all orbits consistent with the "true" orbit. Each set of the sampled orbital elements is referred to as a "clone". Assuming that we have a set of six orbital elements $y_i = (a, e, i, \omega, \Omega, M)$, and they are correlated, the orbital elements for each clone can therefore be written in the form:

$$y_i = y_0 + X_{ik} \Lambda_{kj} \xi_j, \quad (3)$$

where y_0 is 6×1 column vector of the nominal orbital elements of the body, X_{ik} is 6×6 matrix with columns equal to the eigenvectors of the covariance matrix of the orbital elements, Λ_{kj} is a diagonal matrix with elements corresponding to the eigen-values of the covariance matrix and ξ_j is a random number sampled from a normal distribution with mean $\mu = 0$ and standard deviation $\sigma = 1$. Using that approach, we create 1000 clones for each assumed parent body, 96P and P/1999 J6, that is integrated back in time until an epoch for interest.

3.3. Phase 1: backward integrations of parent body candidates

3.3.1. Parent candidate #1 96P/Machholz

The equations of motion of comet 96P and each clone are integrated back in time until 50000BCE, using a force model as described in Section 3.1. The lengthy backward integration (5×10^4 years) was chosen with the aim of encompassing at least a few circulation cycles of the longitude of the ascending node (Ω), allowing us to study the resulting meteoroid streams over a long time period. However, we emphasize that even though our backward integrations extend to 50000 BCE, we only consider meteoroid ejection epochs since 20000 BCE. The reason for that is that the time window of 50 millenia is comparable to the dynamical and physical lifetimes of JFC (e.g., Levison and Duncan, 1994; 1997), so backward integration until 50000 BCE merely aims to illustrate the past evolution of the orbit of 96P.

Our symplectic method (see Section 3.1) uses a fixed integration time step. We chose $\Delta t = 12 \text{ h}$ to balance speed with accuracy. To be more precise, prior to the main integrations, we performed sample simulations in order to determine an optimal time step for both parents 96P and P/1999 J6 where the method is described in detail in Abedin et al. (2017).

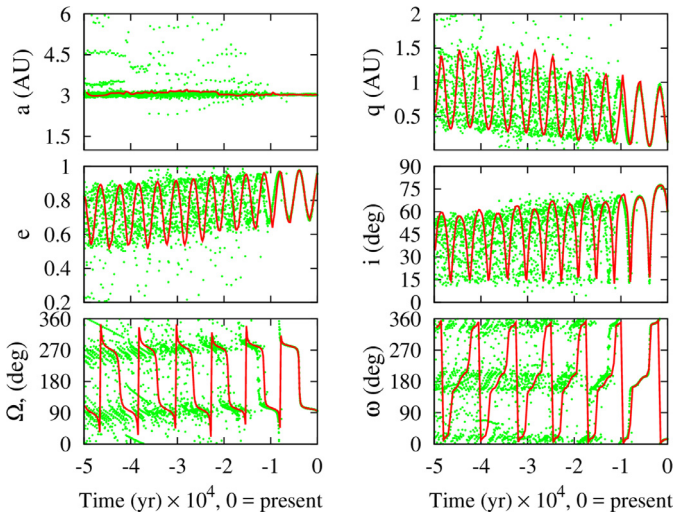


Fig. 3. Backward evolution of the nominal orbital elements of comet 96P/Machholz (red line), along with 10^3 clones (green dots), over 5×10^4 years. (For interpretation of the references to color in this figure legend, the reader is referred to the web version of this article.)

During the backward integrations, we impose a perihelion cut-off distance of $5 R_{\odot}$. Any clone or parent body that approached the Sun below that limit is considered “dead” and removed from the simulations. Comets are unlikely to survive at such short distances from the Sun, which is also evidenced by the disruption of the Kreutz group of sungrazing comets (Sekanina and Chodas, 2005). In fact, the sun grazing stage of the evolution of comets is considered a frequent end state of most comets (e.g., Bailey et al., 1992).

The evolution of the orbital elements of the 1000 clones and the nominal orbit of 96P are presented in Fig. 3. The orbit is stable over a time scale of ~ 7500 years and evolves smoothly, while beyond that time the dispersal of the clones becomes significant. Furthermore, the orbit of 96P/Machholz is in state of Kozai type oscillation, which manifests itself in a distinct correlation between some of the orbital elements. In the Kozai-type orbital evolution, the semi-major axis of the orbit is approximately conserved while there is out-of-phase oscillation of the perihelion distance, eccentricity and inclination of the orbit. That is, when the orbital inclination is at its maximum value $i \approx 80^\circ$, the orbital eccentricity reaches a minimum $e \approx 0.7$, while the perihelion distance is also at its maximum value $q \approx 1$ AU. Conversely, when the inclination is at minimum $i \approx 15^\circ$, the eccentricity is at its maximum ($e \approx 0.99$) while the perihelion distance reaches a minimum value of $q \approx 0.05$ AU. This oscillation in (e , i , q) for 96P occurs with a period of ≈ 4100 years, whereas the longitude of the ascending node (Ω) and the argument of perihelion (ω) circulate from 0° to 360° , with a period of ≈ 8200 years (see Fig. 3). The fact that the orbit of 96P is in a state of Kozai-type oscillation will be used for selecting clones for meteoroid ejection in Section 3.4.1.

3.3.2. Parent candidate #2 P/1999 J6

Using the approach outlined in Section 3.2.1, we created 1000 clones sampled from the 6-dimensional phase space of the nominal orbital elements of P/1999 J6. Then the orbits of the clones were integrated backwards in time until OCE. This time span is motivated by the hypothesis that the Marsden group of comets, and the ARI, SDA and NDA showers may have formed between 100–950 CE (Sekanina and Chodas, 2005). In order to encompass the suggested comet breakup time interval, the earliest of these epochs (100 CE) will be used for the meteoroid ejection onset time from P/1999 J6 and forward integrations of their orbits.

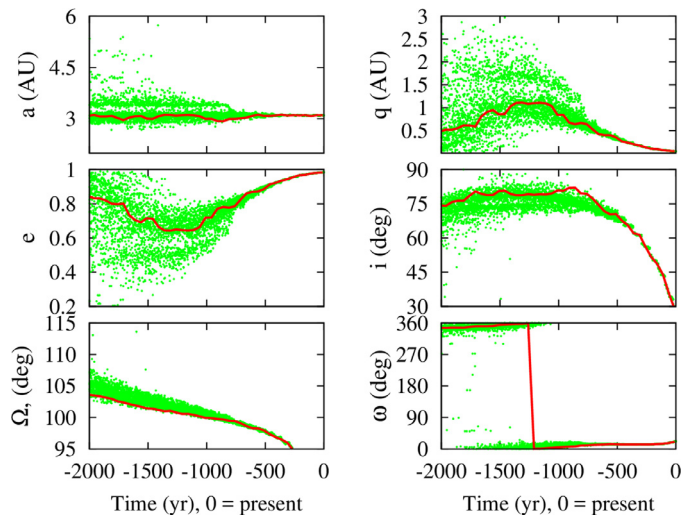


Fig. 4. Backward evolution of the nominal orbital elements of comet P/1999 J6 (red line), along with 10^3 clones (green dots), over 2000 years. (For interpretation of the references to color in this figure legend, the reader is referred to the web version of this article.)

For the backward integration of the orbit of P/1999 J6, we found an optimum fixed time step of $\Delta t = 4$ h, utilizing the force model as described in Section 3.1. We note the shorter integration time step used for the orbit of P/1999 J6 compared to $\Delta t = 12$ h for 96P. The reason for that is P/1999 J6 experiences more shallow and frequent encounters with Jupiter, so time step of at least $\Delta t = 4$ h is needed in order to smoothly sample its motion around the Sun.

The result from the backward integrations are presented in Fig. 4. The orbit of P/1999 J6 quickly becomes chaotic after only 500 years, owing to frequent close encounters with Jupiter. The onset of chaos was verified by Lyapunov exponent calculations, and corresponds in Fig. 4 to the time where the orbital elements begin to spread significantly. Presently, the perihelion distance of the comet reaches its minimum distance of $q \approx 0.05$ AU, while the eccentricity is almost at its maximum value of $e \approx 0.98$ (see Fig. 4). The present value of the inclination is $i \approx 26.6^\circ$ but only 1.5 millennia ago it was about $i \approx 75^\circ$, where the perihelion distance was at its maximum value of $q \approx 1$ AU.

Due to the quick dispersal of the clones of P/1999 J6, it becomes difficult to know the true orbit of the comet prior to 100 CE due to chaos. However a careful selection of clones using the past evolution of P/1999 J6 could still provide meaningful results from the forward simulations.

3.4. Phase2: Forward integration

3.4.1. Selection of “clones” for meteoroid ejection from parent candidate #1: 96P/Machholz

We use the fact that the orbit of 96P is in state of Kozai oscillation in order to select clones for meteoroid ejection and forward integrations. This type of secular evolution approximately conserves the Kozai energy (e.g., Kozai, 1962; Kinoshita and Nakai, 1999) which can be expressed as

$$C = (2 + 3e^2)(3 \cos^2 i - 1) + 15e^2 \sin^2 i \cos 2\omega, \quad (4)$$

where e is the eccentricity, i is the inclination and ω is the argument of perihelion of the orbit respectively. Over the period of interest here (22000 years in the past) the argument of perihelion (ω) would have completed roughly 3 precession cycles, indicating that 96P’s osculating value of ω can take any value between 0° and 360° , whereas the eccentricity of the orbit would lie between $e \sim 0.7 - 0.97$. However, due to the correlation between e and ω ,

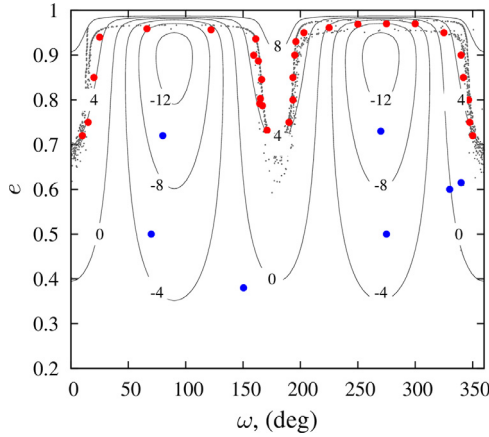


Fig. 5. Snapshot of the Kozai evolution of the orbit of 96P/Machholz in 20000 BCE for different values of the Kozai energy C . The grey dots denote all the clones, superimposed over the trajectories of constant C , where the red dots indicate “good” clones, that we select for meteoroid ejection and forward integrations. Examples of “bad” clones that are discarded in our simulations are denoted with blue dots. (For interpretation of the references to color in this figure legend, the reader is referred to the web version of this article.)

the actual values that the orbit of 96P can take are constrained to a curve called the *Kozai trajectory* for a given value of the Kozai energy C . Fig. 5 shows the Kozai trajectories for the nominal orbit of 96P/Machholz, in $(e - \omega)$ space for different values of the Kozai energy C . In addition, the orbital elements of all clones of 96P for the epoch of 20000 BCE are mapped.

It is evident from Fig. 5 that the Kozai energy for 96P/Machholz is not strictly conserved, owing to the fact that close approaches to Jupiter and planetary perturbations are not considered in the Kozai formalism. Nevertheless, using the information of an approximate conservation of C provides vital information about the appropriate selection of clones for forward simulations. That is, during the secular evolution of the orbit of 96P, we expect that the true orbit must lie on or near a Kozai trajectory for $C = 4$. We thus sample our clones for forward integrations along that trajectory (see Fig. 5 for details). Ideally, one would select as many clones as possible, covering the entire range of argument of perihelion (ω) and eccentricity (e). However, here we sample only 10 clones due to the lengthy integrations times. The sampled clones are equally spaced in the range of $\omega = 0^\circ - 360^\circ$, while covering the interval $e = 0.7 - 0.97$.

3.4.2. Selection of “clones” for meteoroid ejection from parent candidate #2: P/1999 J6

Assuming that the primary reason for the dispersal of the clones is close planetary encounters, we chose to select clones that are situated close to the nominal orbit of the comet. The reason for that is that clones that lie far from the orbit can not end up on the present orbit of comet P/1999J6 and thus produce the observed characteristics of the resulting meteor showers (i.e. location of peak activity and spread, radiant location, geocentric speed etc.). Such an occurrence would require that all or nearly all of the ejected meteoroids suffer planetary encounters that place them on the present orbits of the observable streams, which cannot happen in practice due to the stochastic nature of planetary encounters.

Using the argument discussed above, we select 10 clones near the nominal orbit of P/1999 J6. Clones “near” the nominal orbit are considered to be those with orbital elements differing by no more than 1% of the orbital elements of P/1999 J6. That should ensure that meteoroids ejected from these clones end up in or

close to the phase space of orbital elements of those meteoroids presently intersecting the Earth.

3.4.3. Orbit integration of meteoroids ejected from parent candidate #1 96P/Machholz

Using the approach outlined in Section 3.2, 3000 meteoroids are ejected at every 10 perihelion passages (or roughly every 55 years) from ten suitable clones, over an arc assuming the comet activity turns on at a heliocentric distance of $r \leq 3$ AU. That distance roughly corresponds to the threshold at which the water ice begins to sublimate (Delsemme, 1982). Assuming the orbital period of 96P (≈ 5.5 years) does not vary dramatically, and the meteoroid ejection onset is ~ 20000 BCE, that roughly corresponds to meteoroid ejection over ~ 400 perihelion returns until the present. This amounts in $\sim 1.2 \times 10^6$ particles per clone, in the range of their radii $s = 100 \mu\text{m} - 1$ mm.

Similar to the backward integrations, the equations of motion of the ejected meteoroids are integrated forward in time with a fixed time step of $\Delta t = 12$ h, until the present. Furthermore, a perihelion cut-off distance of 0.025 AU or $5R_\odot$ is imposed, so meteoroids below that limit are removed from further integrations. Moreover, only meteoroids having their orbital nodes within 0.01 AU (a “sieve” distance) from the Earth’s orbit are considered as capable of producing a shower at the Earth. In reality, only meteoroids actually hitting the Earth can be observed as meteors, however due to the unrealistically low number of the simulated meteoroids, a nodal distance of 0.01 AU seems a good compromise.

3.4.4. Orbit integration of meteoroids ejected from parent candidate #1 P/1999 J6

Due to the shorter time-scales of integrations here (only 2000 years), 3000 meteoroids are ejected from 10 clones of P/1999J6 every fifth perihelion return (or approximately every 27 years), so that approximately the same (compared to 96P) dust production ($\sim 1.2 \times 10^6$ particles per clone) is maintained. That results in 73 active perihelion returns of each clone. Finally, the only remaining difference here is that we use a shorter integration time step of $\Delta t = 4$ h (as for the backward simulations), due to more frequent encounters of P/1999J6 with Jupiter. All other parameters such as comet activity turn-on distance, perihelion cut-off distance and meteoroid sieve distance are the same as in Section 3.4.3.

3.4.5. Weighting of meteoroids by their perihelion distance at time of ejection

The comet’s sublimation rate decreases with heliocentric distance (e.g., Sekanina, 1988; 1992) and is a non-linear process. As a comet approaches the Sun, sublimation becomes more violent, which increases the dust production rate (Schulz, 2006) and the meteoroid ejection speeds (Whipple, 1950; 1951; Brown and Jones, 1998). Thus, the number of meteoroids will be dependent on the perihelion distance of the parent at the time of ejection. We use a weighting scheme suggested by Jones (2002), given as:

$$W_s = \frac{\theta_c(1-e)^2}{q^2\sqrt{1-e^2}} \quad (5)$$

where

$$\theta_c = \arccos\left(\frac{q(1+e) - r_0}{r_0 e}\right) \quad (6)$$

is the true anomaly corresponding to the comet-Sun distance r_0 in AU, at which the cometary activity turns on, e is the orbital eccentricity and q is the perihelion distance in AU. In the weighting process we set $r_0 = 3$ AU throughout. It is well known that more volatile components such as, CO and CO₂ begin to sublimate at much larger heliocentric distances e.g., as large as $r_0 \approx 5$ AU (see

Sekanina, 1988), but it is unlikely that the gas pressure can lift millimeter size particles off the comet's surface.

Using the weighting scheme given by Eq. (3.4.5) each particle is assigned a weight, depending on the perihelion distance of the parent at the time the meteoroid is ejected. For example, a meteoroid ejected from a parent with a perihelion distance of 1 AU and an eccentricity of $e=0.96$, assuming $r_0=3$ AU will be weighted by $W_s \approx 6$, whereas a particle released from a parent with a perihelion distance of $q=0.1$ AU and the same eccentricity (orbit size and shape similar to 96P/Machholz) will be weighted by $W_s \approx 340$. Thus, this weighting will be used to correct the meteoroids' number distribution.

3.4.6. Weighting by meteoroid size

In Section 3.2 we mentioned that the ejected meteoroids in our simulations are sampled from a size distribution which is flat in the logarithm of particles' size, in the range 100 μm –1 mm, equivalent to radar and optical meteors respectively. However, this size distribution is not realistic. Generally, more particles are released at smaller sizes compared to larger ones, which is evidenced from meteor observations. Following Wiegert et al. (2009), this flat size distribution can be calibrated to a differential size distribution as $dN/dr = r^\alpha$. The weighting that needs to be applied to account for differential size distribution is just $W_r = r^{\alpha+1}$.

The observed sized distribution of meteors can roughly be approximated with a power-law as $dN(m) \propto m^{-s} dm$, where $s \sim 2.34$ (see Whipple, 1967; Grun et al., 1985) is referred to as *mass index* of the distribution. Since $m \propto r^3$, then $dN(r) \propto r^{-3s+2} dr \approx r^{-5} dr$. Thus, the needed weighting to correct for the meteors' size distribution is $W_r \approx r^{-3s+3} \approx r^{-4}$. Finally, the total weighting that is needed to be applied to the meteors in order to account for a realistic meteor number distribution, will be the product of the weightings due to the particles' perihelion distance at time of ejection and particle size distribution, namely $W_{tot} = W_s W_r$.

4. Results

In this section we present the results of the simulated meteoroid streams of both parent candidates, 96P and P/1999 J6, and compare the characteristics of their resulting showers with wide range of meteor observations e.g., radar (CMOR and SAAMER), optical (CAMS) and visual (IMO) surveys. We first examine the simulation-observation fits for each individual meteor shower, produced by each individual parent candidate and then provide a qualitative comparison of their combined contribution to the common showers.

For the sake of brevity, we present results for only one clone for each parent body, the clone which produces the best fit in our simulations. Moreover, we show the results of the single initial meteoroid ejection onset time which yields the best match. However, snapshots of the fits for every 1000 years, between 20000 BCE and the present, are presented in the on-line Supplementary Material (SM). All our results are presented only for meteoroids that approach the Earth's orbit within 0.01 AU i.e., for meteoroids considered to produce meteors.

The width of the activity profile is a rough proxy as to the age of a meteor shower. We use that information and attempt to simultaneously fit the observed widths and peak location of all resulting showers, from each parent body, in order to obtain a self-consistent scenario of the age and formation mechanism of the meteoroid complex of 96P.

Finally, we omit the results for the Arietids that were investigated in a previous work (Abedin et al., 2017). However, in Section 5 we provide a brief discussion as to how the results of that work fit in the context of the present study.

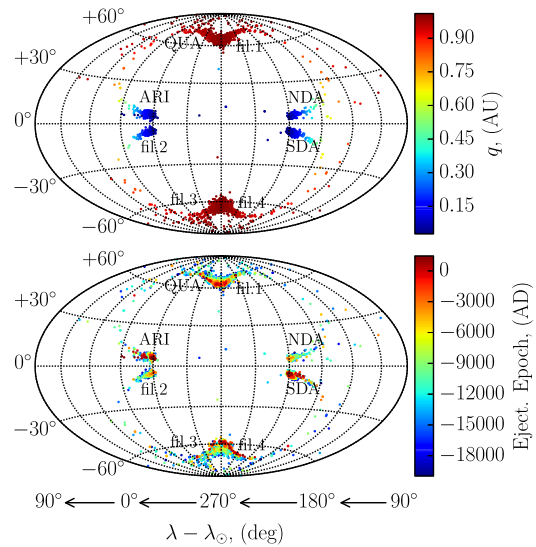


Fig. 6. Resulting radiant distribution of meteoroids ejected from a single clone of comet 96P with a meteoroid ejection onset time 20000 BCE. The radiants in the top panel are color coded in terms of meteoroids' present perihelion distance, and as a function of meteoroid ejection epoch (lower panel). (For interpretation of the references to color in this figure legend, the reader is referred to the web version of this article.)

4.1. The simulated meteor showers of parent candidate - 96P/Machholz

Assuming that 20000 BCE is the initial meteoroid ejection onset time, the longitude of the ascending node and argument of perihelion of the orbit of 96P will complete approximately 2.5 Kozai circulation cycles, causing the ejected meteoroids to intersect the Earth's orbit at 8 different locations (cf. Fig. 1 in Section 2). That results in 8 different meteor showers to be detected on the Earth, as originally suggested by Babadzhanov and Oubrov (1992). Fig. 6 shows the simulated shower radiants. Four of these showers, QUA, ARI, SDA and NDA were identified by Babadzhanov and Oubrov (1992) and are well known. The remaining four showers, which we call "filaments", have relatively recently been identified as showers. The Quadrantids and filament 1 are part of the northern toroidal source (Brown et al., 2010; Jenniskens et al., 2016), whereas filament 2 is the southern branch of the ARI and contributes to the helion sporadic source (Brown et al., 2008). The SDA and NDA are part of the anti-helion sporadic source (e.g., Brown et al., 2010; Jenniskens et al., 2016), while filaments 3 and 4 are found in the southern toroidal source (Pokorný et al., 2017).

An interesting feature is the clear correlation between the perihelion distance and the showers' radiants (Fig. 6). The toroidal showers have perihelion close to 1 AU, and the intersection with the Earth's orbit occurs close to that point. The ecliptic showers, on the other hand, are in a sunskirting state approaching the Sun as close as 0.025 AU or slightly farther than $5R_\odot$. Fig. 6 shows that there is no strong correlation between the showers' radiants and the meteoroid ejection epoch, though it is evident that cores of some of the showers are dominated by younger particles.

4.1.1. The Quadrantids (QUA)

In Abedin et al. (2015) we investigated the Quadrantid meteoroid stream. We demonstrated that the age of the central part of the stream is only 200 years old and is associated with asteroid 2003 EH₁. We also showed that the wings of the activity profile must be much older and are associated with comet 96P. These results had been suggested by several previous studies

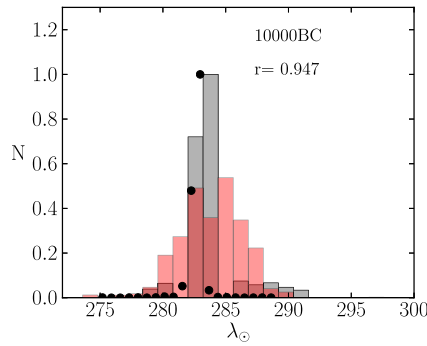


Fig. 7. Simulated, weighted and normalized activity profile (red histogram) of the QUA, originating from 96P/Machholz with meteoroid ejection onset in 10000 BCE. Superimposed are the observed normalized relative activity profiles by CMOR (grey histogram) and IMO visual observations (black circles). The quantity r denotes the sum of the residuals of the fit between the theoretical and CMOR profile. (For interpretation of the references to color in this figure legend, the reader is referred to the web version of this article.)

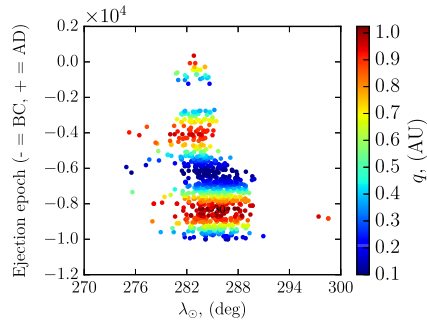


Fig. 8. Solar longitude distribution of QUAs as a function of meteoroid ejection epoch, from comet 96P/Machholz assuming meteoroid ejection onset in 10000 BCE. Individual meteoroids are color coded in terms of their perihelion distance at time of ejection. (For interpretation of the references to color in this figure legend, the reader is referred to the web version of this article.)

(e.g., Jenniskens, 2004; Wiegert and Brown, 2005; Neslušan et al., 2013a). However, in the current work we will mainly concern ourselves with the broader (long-lasting) component of the QUA, associated with 96P.

Fig. 7 shows the simulated weighted activity profile of the QUA, assuming meteoroid ejection from comet 96P with initial onset epoch in 10000 BCE. The location of the peak of the activity profile produced a good match with the CMOR and IMO visual observations, though the simulated *Full Width of Half Maximum* FWHM ≈ 6 days was significantly wider. Fig. 8 shows the simulated distribution of meteoroids, presently reaching the Earth, as a function of their ejection epoch and perihelion distance at that epoch. The perihelion distance of 96P was low between 7000 BCE and 5000 BCE, so meteoroids released within that time frame are weighted more, which is the reason for the presently wider FWHM. The poor match between the simulated and observed peak of the QUA is not surprising, as the contribution of asteroid 2003 EH₁ is not considered here, and whose ejecta were shown to dominate the core of the stream (Abedin et al., 2015). That results in a very narrow peak activity consisting of relatively large meteoroids, while the extended moderate activity is associated with 96P.

Our interest here is in the wings of the activity profile which produce a relatively good match to the CMOR observations. Brown et al. (2010) argued that QUA show significant low level activity in the range $232^\circ < \lambda_\odot < 270^\circ$, which was also predicted by simulations. However, we find that the long-lived activity identified by Brown et al. (2010), as part of the QUA may result from two weak nearby showers that peak in the range $232^\circ < \lambda_\odot < 260^\circ$ and partially overlap with the wings of the QUA (see Section 4.1.4).

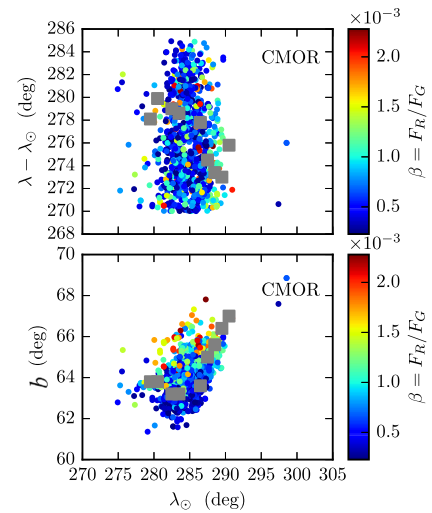


Fig. 9. Simulated sun-centered radiant drift of QUA, with assumed meteoroid ejection onset in 10000 BCE from comet 96P. The color coding is in terms of meteoroid size. Superimposed is the observed radiant drift by CMOR (grey squares). (For interpretation of the references to color in this figure legend, the reader is referred to the web version of this article.)

The simulated radiant drift of the QUA is presented in Fig. 9, superimposed over the measurements by CMOR. The simulated mean radiant position at the peak activity $\lambda_\odot = 283.5^\circ$ was $\lambda - \lambda_\odot = 276.4^\circ \pm 3.9^\circ$ and $b = 63.8^\circ \pm 0.9^\circ$, which translates in a mean difference with the CMOR radiant of approximately 0.8° . Our simulations indicate that the QUA stream seems to be mainly dominated by relatively old ejecta (prior to 3000 BCE) (see Fig. 8) and mostly comprised of small β meteoroids. The reason for that may be the 2:1 mean-motion resonance with Jupiter (e.g., Hughes et al., 1981; Froeschle and Scholl, 1986; Gonczi et al., 1992; Wiegert and Brown, 2005), which has perhaps scattered away most of the smaller component of the stream, preferentially leaving larger meteoroids. We note that the mean semi-major axis of the stream places it just outside of the 2:1 mean-motion resonance (Froeschle and Scholl, 1986; Wiegert and Brown, 2005). Also, solar radiation pressure increases the size of the orbits of smaller meteoroids. This affects the location of mean-motion resonances, and may even bring them to Jupiter-intersecting orbits, resulting in scattering.

Fig. 10 shows the distribution of the orbital elements of the QUA, assuming meteoroid ejection onset circa 10000 BCE from comet 96P, as a function of the solar longitude λ_\odot . The simulated orbital elements yield a good match to the measurements by CMOR and CAMS, even though the contribution of asteroid 2003 EH₁ has been omitted here. The fit of our simulations to the observations suggests that the wings of the QUA can be explained by continuous cometary activity of 96P over the last 12,000 years, which renders the current age estimate significantly higher than previous estimates of 2200–8000 years (Gonczi et al., 1992; Jones and Jones, 1993; Williams and Wu, 1993; Neslušan et al., 2013b).

4.1.2. The Southern δ -Aquariids (SDA)

The simulated activity profile of the SDAs originating from 96P and assuming a meteoroid ejection onset time in 17000 BCE, is presented in Fig. 11 and compared to the observed activity profiles by CMOR and IMO. We recall that we show the simulated resulting shower characteristics only for the meteoroid ejection epoch that produces the best match (see Section 4). Older or earlier ejecta produce poorer fits to the observations. Fig. 12 shows the nodal longitude of the meteoroids presently approaching the Earth's orbit within 0.01 AU, as a function of their ejection epoch and perihelion distance at the time of ejection. It is evident that the meteoroids primarily contributing to the peak of the profile are

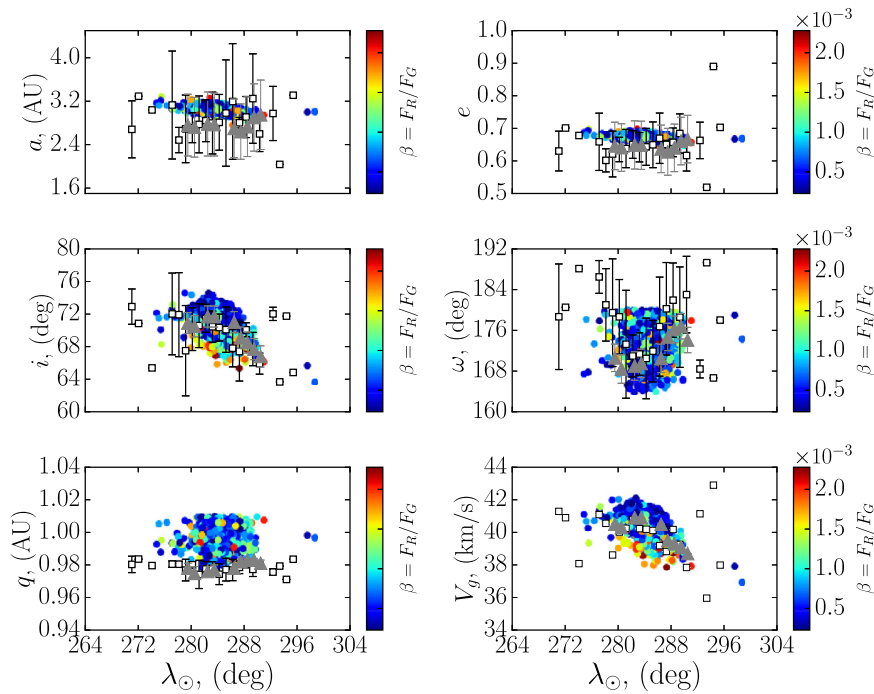


Fig. 10. Simulated distribution of the orbital elements of the QUA (color dots) for assumed meteoroid ejection onset epoch in 10000 BCE from comet 96P. The color coding is in terms of the meteoroids' β -parameter (equivalent to meteoroid size). Superimposed are the observed distributions by CAMS (open squares) and CMOR (grey triangles). (For interpretation of the references to color in this figure legend, the reader is referred to the web version of this article.)

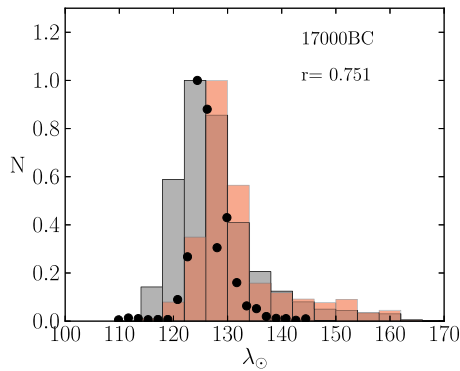


Fig. 11. Simulated, weighted and normalized activity profile (red histogram) of the SDA, originating from 96P/Machholz with meteoroid ejection onset in 17000 BCE. Superimposed are the observed normalized relative activity profiles by CMOR (grey histogram) and IMO visual observations (black circles). Details similar to Fig. 7. (For interpretation of the references to color in this figure legend, the reader is referred to the web version of this article.)

those ejected circa 2000 BCE and 6000 BCE. Particles older than 10000 BCE contribute mainly to the wings of the profile.

Overall, the peak location and the width of the wings of the activity profile yielded a good match to the observation. The FWHM is somewhat narrower than observed but significantly improves when the contribution of comet P/1999 J6 is added (Section 4.2.1). The sum of the residuals begins to deteriorate for particles released after 17000 BCE, resulting in a too narrow profile, inconsistent with the observations. Conversely, ejections older than 17000 BC produce activity of longer duration than found from observations.

The predicted mean radiant position of the SDA at the simulated peak activity $\lambda_{\odot} = 125^{\circ}$ was $\lambda - \lambda_{\odot} = 208.8^{\circ} \pm 0.5^{\circ}$ and $b = -6.9^{\circ} \pm 0.6^{\circ}$. That results in a mean radiant difference of 1.2° compared to CMOR observations. It is worth noting that the CMOR

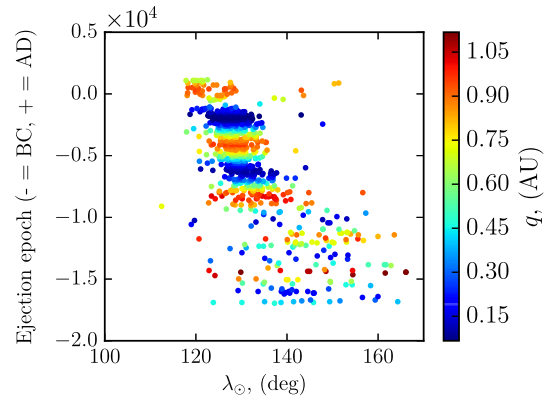


Fig. 12. Solar longitude distribution of SDA as a function of meteoroid ejection epoch from comet 96P/Machholz assuming meteoroid ejection onset in 17000 BCE. Individual meteoroids are color coded in terms of their perihelion distance at time of ejection. (For interpretation of the references to color in this figure legend, the reader is referred to the web version of this article.)

observed radiant has a significant spread as well (of order $2\text{--}3^{\circ}$) due to measurement uncertainties.

The simulated radiant drift is presented in Fig. 13. It shows a significant spread of $\Delta(\lambda - \lambda_{\odot}) \approx 15^{\circ}$, along the ecliptic, but only a moderate dispersal in ecliptic latitude b . In contrast, the CMOR observations measure a nearly constant b for $140^{\circ} < \lambda_{\odot} < 165^{\circ}$, which was not reproduced by our simulations. A possible reason for that may be that there is another body (or bodies) that may be contributing to the SDAs that has not been accounted for in the current study. In fact, beside comet 96P and P/1999 J6, Neslušan et al. (2013a) showed that asteroid 2003 EH₁ also contributes to the SDAs. Nevertheless, meteoroid ejections from 96P, circa 17000 BCE produce a good match to the observed characteristics of the SDAs, in particular the duration of the shower activity.

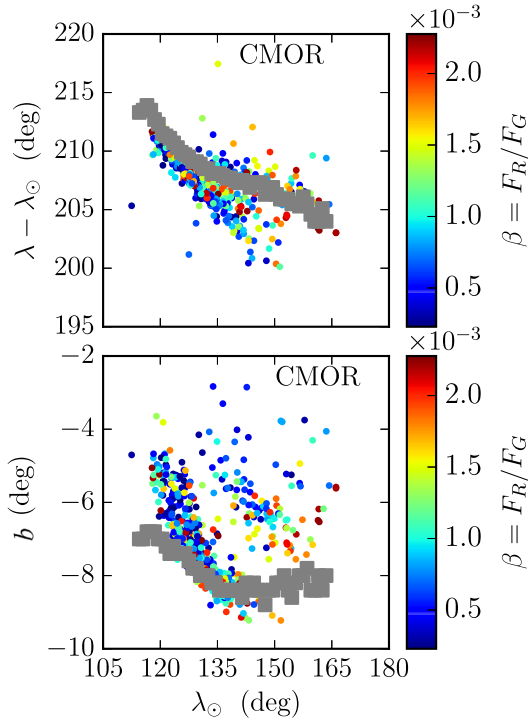


Fig. 13. Simulated sun-centered radiant drift of SDA, with assumed meteoroid ejection onset in 17000 BCE from comet 96P. The color coding is in terms of meteoroid size. Superimposed is the observed radiant drift by CMOR (grey squares). (For interpretation of the references to color in this figure legend, the reader is referred to the web version of this article.)

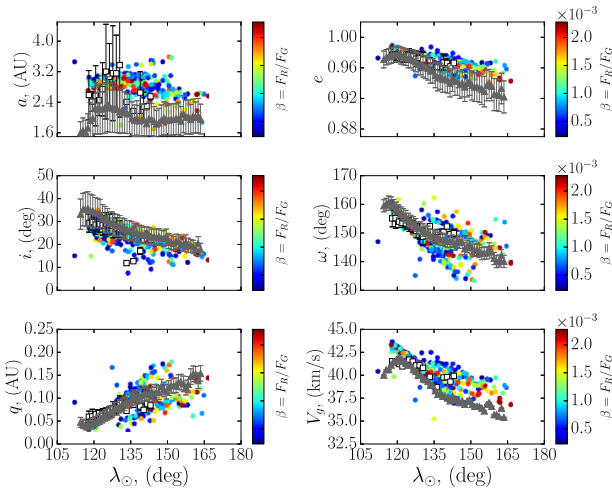


Fig. 14. Simulated distribution of the orbital elements of the SDAs (color dots) for assumed meteoroid ejection onset epoch in 17000 BCE, from comet 96P. The color coding is in terms of meteoroids' β -parameter (equivalent to meteoroid size). Superimposed are the observed mean values of the orbital elements in each bin, respectively by CAMS (open squares) and CMOR (grey triangles). The error bars correspond to 1σ uncertainty. (For interpretation of the references to color in this figure legend, the reader is referred to the web version of this article.)

Fig. 14 shows the simulated distribution of the orbital elements of the SDAs as a function of solar longitude, for meteoroid ejection onset in 17000 BCE. The theoretical values are compared against the observations by the CMOR and CAMS meteor surveys. There has been a long-standing discrepancy of the meteoroids' calculated orbital semi-major axis and geocentric speeds derived from optical and radar surveys (Jenniskens et al., 2012). It is evident that the meteoroids' semi-major axes deduced from radar measurements are systematically lower than the optical measurements. Some-

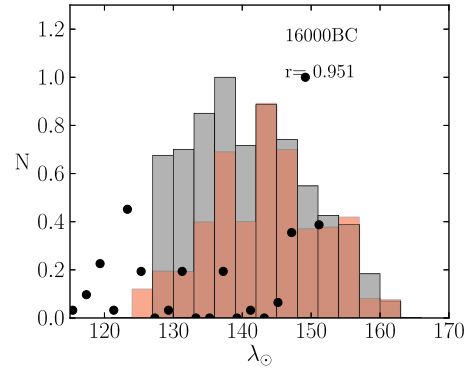


Fig. 15. Simulated, weighted and normalized activity profile (red histogram) of the NDA, originating from 96P/Machholz with meteoroid ejection onset in 16000 BCE. Superimposed are the observed normalized relative activity profiles by CMOR (grey histogram) and IMO visual observations (black circles). Details similar to Fig. 7. (For interpretation of the references to color in this figure legend, the reader is referred to the web version of this article.)

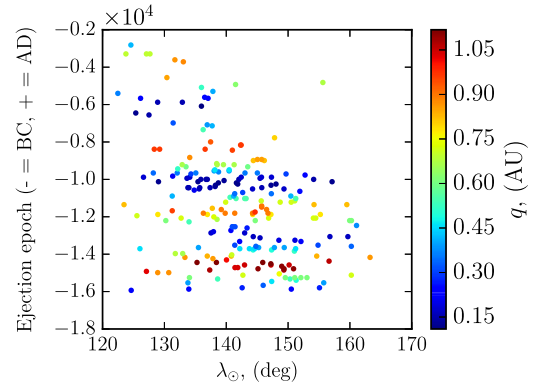


Fig. 16. Solar longitude distribution of NDA as a function of meteoroid ejection epoch, from comet 96P/Machholz. Individual meteoroids are color coded in terms of their perihelion distance at time of ejection. (For interpretation of the references to color in this figure legend, the reader is referred to the web version of this article.)

times, these differences are larger than the scatter of individual meteoroids. Jenniskens et al. (2012) suggested that the discrepancy is likely due to improper accounting for the atmospheric deceleration of radar size particles. Apart from these discrepancies, the rest of the simulated orbital elements produced a relatively good match to both radar and optical measurements.

4.1.3. The Northern δ -Aquariids (NDA)

The NDAs are the northern branch of the SDAs and are also found in the anti-helion sporadic source. The simulated activity profile of the NDAs is presented in Fig. 15 for meteoroid ejection onset time in 16000 BCE, and compared to observed ones by CMOR and IMO. Fig. 16 shows which particles have been ejected at lower perihelion distances (those meteoroids will receive larger weights) and at what epoch (Sections 3.4.5 and 3.4.6). Our simulations show that the bulk of the meteoroids contributing to the NDAs were released prior to 10000 BCE and the resulting FWHM of the activity profile is wider, compared to the SDAs for example, mainly due to the ejections between 10000 BCE and 14000 BCE.

Fig. 15 shows that the IMO visual observations are rather scattered, without a clear peak. That is mainly due to the weak nature of the NDAs and the preferential detection of only the larger meteoroids by visual observations. In contrast, the radar measurements yielded a better defined overall profile, though also without a clearly distinct peak. Instead, the CMOR profile shows an almost constant activity in the range $130^\circ < \lambda_\odot < 145^\circ$ with a

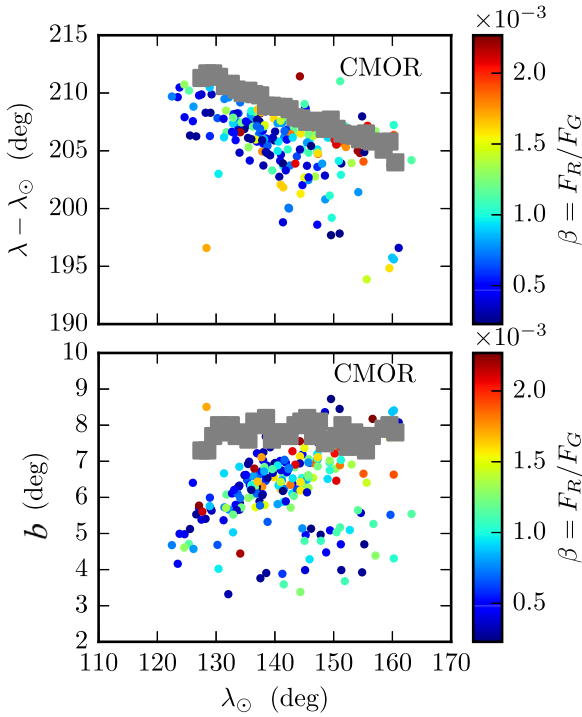


Fig. 17. Simulated sun-centered radiant drift of NDA, with assumed meteoroid ejection onset in 16000 BCE from comet 96P. The color coding is in terms of meteoroid size. Superimposed is the observed radiant drift by CMOR (grey squares). (For interpretation of the references to color in this figure legend, the reader is referred to the web version of this article.)

local maximum around $\lambda_{\odot}=137^{\circ}$. In comparison, our simulated profile yielded a slightly better defined shape and peak, though the latter seems to occur near $\lambda_{\odot}=140^{\circ}$. Overall, the simulated width of the activity profile produced a good fit to the CMOR data. There may be other bodies (not included in this study) also contributing to the NDAs. Nonetheless, our analysis of the fit between the theoretical and observed activity profiles suggest that the shower is much older than the 2000 years previously suggested by [Sekanina and Chodas \(2005\)](#).

The simulated mean radiant location at $\lambda_{\odot}=140^{\circ}$ is $\lambda - \lambda_{\odot} = 206.0^{\circ} \pm 1.4^{\circ}$ and $b = 6.7^{\circ} \pm 0.4^{\circ}$, with a difference of 2.5° from the CMOR measured mean radiant (see [Table 1](#) in [Section 2](#) for details). The simulated radiant drift is presented in [Fig. 17](#) and is compared to the CMOR observations. The simulation yielded satisfactory results, given the uncertainties and the assumptions used in the radiant computation. CMOR measures a substantial drift of almost $\Delta(\lambda - \lambda_{\odot}) = 10^{\circ}$ along the ecliptic but almost none along the ecliptic latitude b . Our simulations produced a poorer fit to the drift along b (see [Fig. 17](#)).

The simulated distribution of the orbital elements of the meteoroids approaching the Earth within 0.01 AU is presented in [Fig. 18](#) and compared with optical and radar observations by CAMS and CMOR, respectively. Similar to previous cases, there is an obvious discrepancy between the simulated and measured semi-major axes and meteoroids' geocentric speeds. Our simulations predict a mean semi-major axis of $a \approx 3$ AU, whereas the radar and CAMS has measured systematically lower values of $a \approx 1.8$ AU. For other showers that we have examined, the optical measurements show larger values for a , though in this case they seem to be in a good agreement with radar data. However, the semi-major axes measured by CAMS show a significant scatter prior to the peak activity, a dispersion comparable to the error bars due to small number statistics. Furthermore, the CAMS measurements are consistent with the semi-major axes calculated by CMOR near and

after the peak. We note that, similar to visual observations, video and TV observations are biased towards larger (millimeter) and faster meteoroids, though the sensitivity threshold is much higher than visual observations. In contrast, aside from the capability of detecting smaller and slower meteors, the radar detections are not limited by the weather conditions and daylight. Thus, it is not unreasonable to expect the CMOR data to be more uniform timewise than the CAMS data.

4.1.4. Filament 1

Our numerical simulations from 96P predicted a meteor shower in the north toroidal source with radiant location between $210^{\circ} < (\lambda - \lambda_{\odot}) < 270^{\circ}$ and $55^{\circ} < b < 70^{\circ}$ with activity period between $220^{\circ} < \lambda_{\odot} < 270^{\circ}$. Using a 3D-Wavelet search, described in [Section 2](#) we have identified two weak showers in the CMOR data that overlap in time ([Fig. 6](#)) and also simultaneously matched, within the uncertainty, the QUA shower. These showers are the November ι -Draconids (NID) and the December α -Draconids (DAD), being identified as separate in the IAU MDC. The simulated activity profile of this filament is presented in [Fig. 19](#), and compared to the CMOR observations. Our simulations suggest that if this filament is considered as a single shower, then its activity steadily increases reaching a maximum activity near $\lambda_{\odot} = 260^{\circ}$ and then suddenly decreases to the sporadic background activity and merges with QUA. However, if the filament indeed consists of two weak nearby showers, their separation is not resolved by the wavelet search, similar to the result reported by [Neslušan et al. \(2013b\)](#). According to [Brown et al. \(2010\)](#), the NIDs are active from $221^{\circ} < \lambda_{\odot} < 267^{\circ}$ with maximum activity near $\lambda_{\odot} = 241^{\circ}$, whereas the CAMS data sets the activity period $239^{\circ} < \lambda_{\odot} < 267^{\circ}$ with a peak activity at $\lambda_{\odot} = 242^{\circ}$ ([Jenniskens et al., 2016](#)). In contrast, the CAMS measured activity period of the DADs is $239^{\circ} < \lambda_{\odot} < 262^{\circ}$ with a maximum activity at $\lambda_{\odot} = 256^{\circ}$ ([Jenniskens et al., 2016](#)). Evidently, the NID and DAD peak at the same time, both eventually merging with early QUA activity. We call these two showers - filament 1. The best match between the CMOR-derived activity profile of filament 1 and our simulations was obtained assuming meteoroid ejection onset time circa 19000 BCE, from comet 96P. Earlier ejections resulted in a too narrow profile and low activity, inconsistent with the CMOR-derived profile. In fact the youngest particles that presently reach the Earth must have been released around 3000 BCE (see [Fig. 20](#)).

Our calculated mean radiant location at the peak activity of $\lambda_{\odot} = 256^{\circ}$ was $\lambda - \lambda_{\odot} = 259.2^{\circ} \pm 18.9^{\circ}$ and $b = 66.7^{\circ} \pm 3.1^{\circ}$. That peak location corresponds to the maximum activity time of the DAD ([Jenniskens et al., 2016](#)), and the comparison with the CAMS radiant results in a mean difference of about 11° ([Section 2, Table 1](#)). That is clearly a poor match with the observations. However, if we calculate the radiant at the peak time of the NID ($\lambda_{\odot} = 242^{\circ}$), then the resulting mean radiant is $\lambda - \lambda_{\odot} = 267.2^{\circ} \pm 8.2^{\circ}$ and $b = 64.1^{\circ} \pm 0.3^{\circ}$, with a mean difference with the CMOR-derived radiant of 2.6° . The overall NID simulated radiant position yielded a better fit to the observations, while the DAD demonstrated a large radiant dispersion which results in a difference of almost 20° with the mean CAMS radiant. However, given the simulation uncertainties and the observational resolution, the NID and DAD appear as a single weak and diffuse shower. In fact, these radiants are quite diffuse in the radar measurements as well. However, we note that the 3D wavelet search applies a speed and radiant probe size, as well as an activity threshold (3σ above the median sporadic background), used to isolate the radiants. That, along with the weak nature are possible reasons of the inseparability of the two showers, or perhaps the NID and DAD are indeed a single continuous shower.

The simulated radiant drift match ([Fig. 21](#)) was also poor. Observations show almost no drift while our simulations predicted

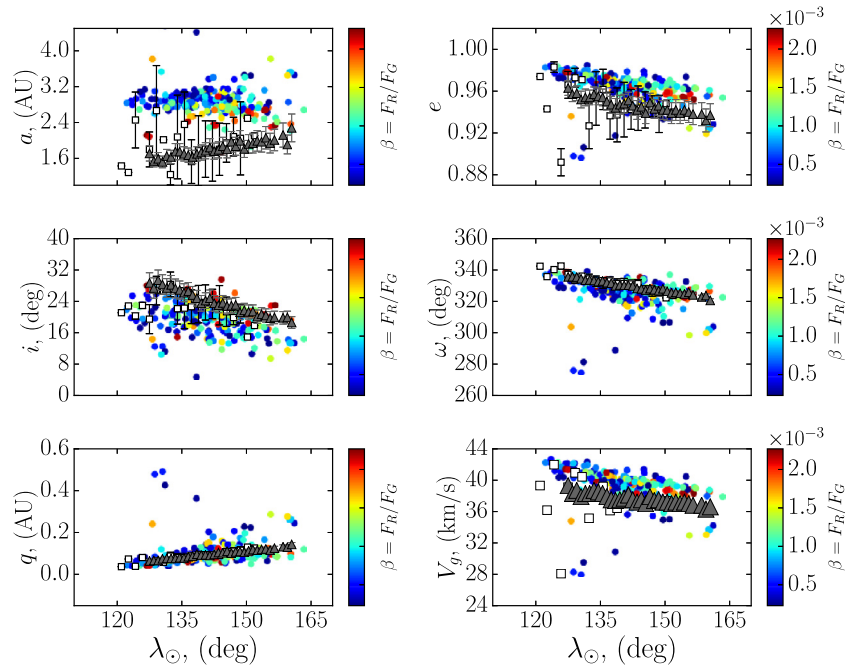


Fig. 18. Simulated distribution of the orbital elements of the NDAs (color dots) for assumed meteoroid ejection onset epoch in 16000 BCE, from comet 96P. The color coding is in terms of meteoroids' β -parameter (equivalent to meteoroid size). Superimposed are the observed distributions by CAMS (open squares) and CMOR (black triangles). (For interpretation of the references to color in this figure legend, the reader is referred to the web version of this article.)

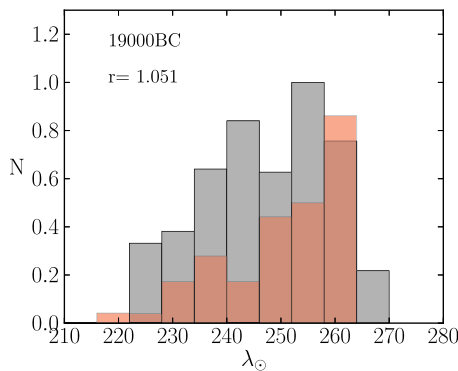


Fig. 19. Simulated, weighted and normalized activity profile (red histogram) of filament 1, originating from 96P/Machholz with meteoroid ejection onset in 19000 BCE. Superimposed is the observed normalized relative activity profiles by CMOR (grey histogram). See Fig. 7 for details. (For interpretation of the references to color in this figure legend, the reader is referred to the web version of this article.)

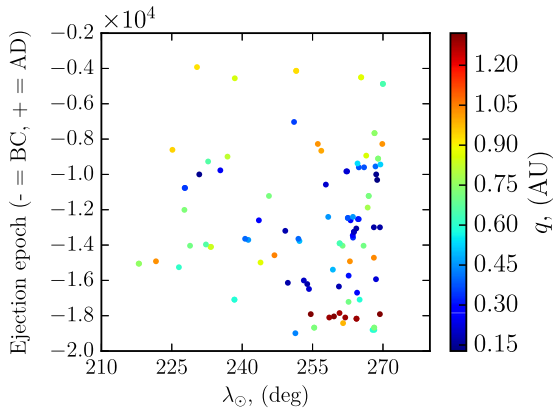


Fig. 20. Solar longitude distribution of filament 1 as a function of meteoroid ejection epoch, from comet 96P/Machholz. Individual meteoroids are color coded in terms of their perihelion distance at time of ejection. (For interpretation of the references to color in this figure legend, the reader is referred to the web version of this article.)

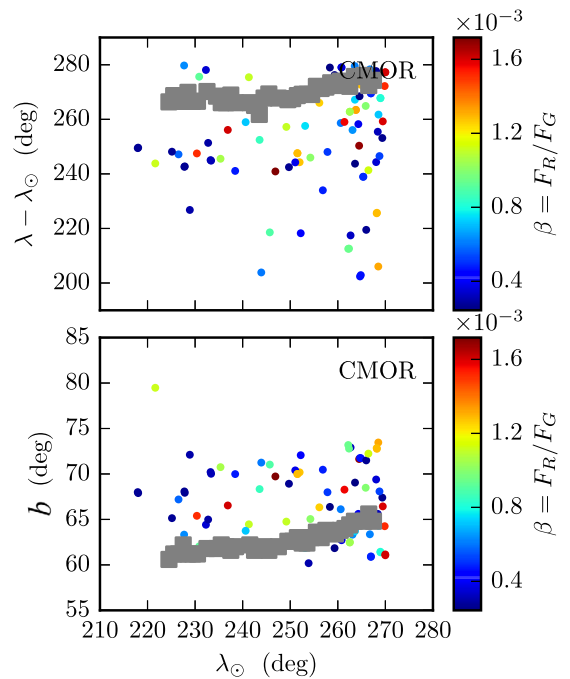


Fig. 21. Simulated sun-centered radiant drift of filament 1, with assumed meteoroid ejection onset in 19000 BCE from comet 96P. The color coding is in terms of meteoroid size. Superimposed is the observed radiant drift by CMOR (grey squares). (For interpretation of the references to color in this figure legend, the reader is referred to the web version of this article.)

a drift of almost $\Delta(\lambda - \lambda_{\odot}) \approx 80^{\circ}$ and $\Delta b \approx 15^{\circ}$. If our simulations represent the past evolution of the complex, its nature is even more complicated than initially thought, where 96P maybe contributes to a few weak nearby showers as well, essentially rendering them a continuous complex of meteoroids whose radiant separation is virtually impossible.

Fig. 22 shows the simulated distribution of the orbital elements of meteoroids, presently reaching the Earth, as a function of the

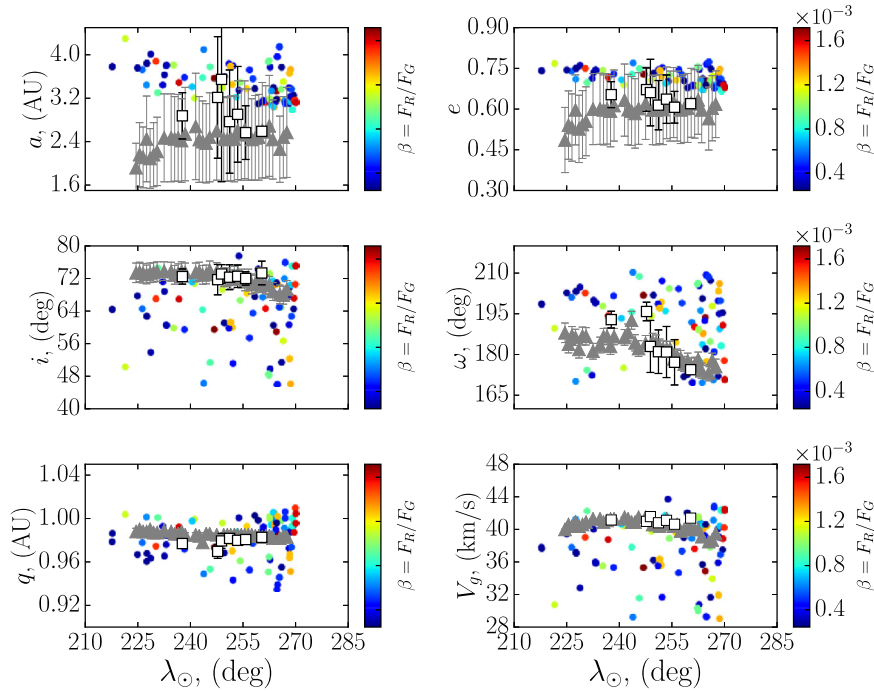


Fig. 22. Simulated distribution of the orbital elements of the filament 1 (color dots) for assumed meteoroid ejection onset epoch in 19000 BCE from comet 96P. The color coding is in terms of meteoroids' β -parameter (equivalent to meteoroid size). Superimposed are the observed distributions by CAMS (open squares) and CMOR (grey triangles). (For interpretation of the references to color in this figure legend, the reader is referred to the web version of this article.)

solar longitude. In addition to the recurring issue whereby CMOR measured speeds tend to produce smaller semi-major axes than the simulations predict, the overall fit to the measured orbital elements was poor. Our simulations predicted a greater scatter in the geocentric speeds and most of the orbital elements between individual meteoroids. The inclination and the argument of perihelion showed a dispersion of almost 20 and 15°, respectively while the theoretical eccentricity was overestimated by approximately 0.15. The poor match of our simulations with the observations may suggest that there is another more dominant parent/parents contributing to filament 1 which was not considered in this work. Conversely, if our simulations represent the past evolution of the 96P complex, that may imply that 96P contributes to a few other meteor showers in the north toroidal source.

4.1.5. Filament 2

Filament 2 in our simulations is predicted to be a meteor shower with radiant location between $325^\circ < (\lambda - \lambda_\odot) < 340^\circ$ and $-10^\circ < b < -4^\circ$ (see Fig. 6), located south of the well known ARI. Using a 3D wavelet search in the CMOR database, we established that filament 2 exists and has an activity profile and radiant position resembling the daytime λ -Taurids (DLTs) (Brown et al., 2008; 2010). Unlike filament 1, the DLTs appear to be stronger and well defined. Fig. 23 shows the simulated activity profile, compared to radar observations by CMOR. The simulated maximum activity occurs at $\lambda_\odot = 82.5^\circ$, while CMOR observations measure a peak activity at $\lambda_\odot = 82.5^\circ$. We note that, to our best knowledge at the time of preparation of this work, there were no reported or available optical observations of the DLT, most likely due to their daytime nature and significantly lower activity compared to the ARI. Investigation of various meteoroid ejection onset times yielded a best match between the theoretical and observed shapes of the activity profiles assuming 96P has been captured in a short period orbit circa 20000 BCE (Fig. 24). However, our residual analysis of the shape of the profiles did not converge to a minimum value, due to our limited simulation time window of 22,000 years.

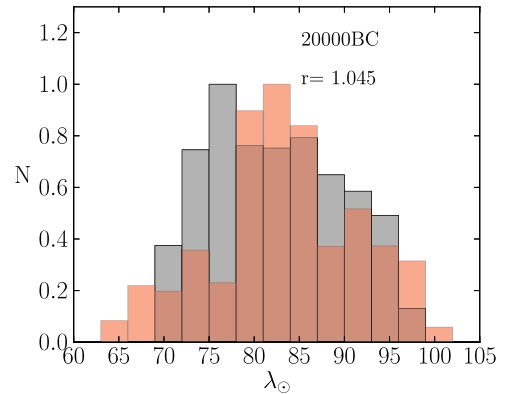


Fig. 23. Simulated, weighted and normalized activity profile (red histogram) of filament 2, originating from 96P/Machholz with meteoroid ejection onset in 20000 BCE. Superimposed are the observed normalized relative activity profiles by CMOR (grey histogram). (For interpretation of the references to color in this figure legend, the reader is referred to the web version of this article.)

That might indicate that the DLTs are even older, or that another body contributes to some portion of the activity profile. We note that there are a few degrees discrepancy between the observed and simulated extent of the wings of the activity profile, likely due to the activity level cutoff threshold of 3σ imposed by our 3D wavelet search (see Section 2). Furthermore, the FWHM of the simulated profile was somewhat narrower compared to the CMOR profile, which leads us to hypothesize that perhaps there may be another body or bodies that may be contributing to the stream, though 96P seems to be the dominant parent.

The simulated mean radiant location at $\lambda_\odot = 82.5^\circ$ was $\lambda - \lambda_\odot = 333.4^\circ \pm 1.3^\circ$ and $b = -6.5^\circ \pm 0.7^\circ$. That corresponds to a mean difference of 2.8° with the CMOR measured mean radiant (see Table 1 in Section 2 for details). Likely, the reason for the small

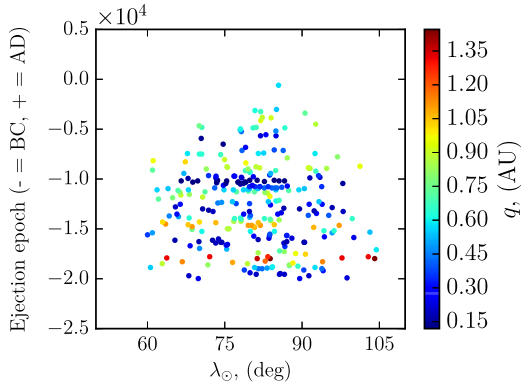


Fig. 24. Solar longitude distribution of filament 2 as a function of meteoroid ejection epoch, from comet 96P/Machholz. Individual meteoroids are color coded in terms of their perihelion distance at time of ejection. (For interpretation of the references to color in this figure legend, the reader is referred to the web version of this article.)

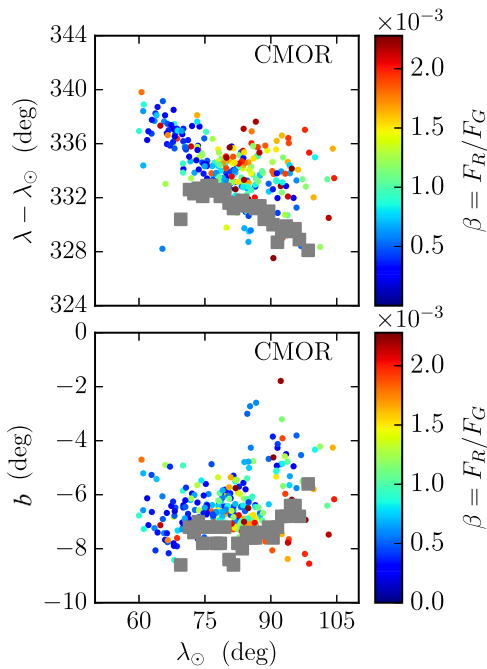


Fig. 25. Simulated sun-centered radiant drift of filament 2, with assumed meteoroid ejection onset in 20000 BCE from comet 96P. The color coding is in terms of meteoroid size. Superimposed is the observed radiant drift by CMOR (grey squares). (For interpretation of the references to color in this figure legend, the reader is referred to the web version of this article.)

difference is the slightly different CMOR-derived peak location, as well as the uncertainties in our simulations.

Fig. 25 shows the simulated radiant drift of the DLTs compared to the CMOR observations. The latter suggests a drift along the ecliptic of $\Delta(\lambda - \lambda_{\odot}) \approx 5^{\circ}$ whereas the simulations yielded $\Delta(\lambda - \lambda_{\odot}) \approx 12^{\circ}$ with slightly larger dispersion. The drift along the ecliptic latitude produced a better match, though the individual radiant drifts also demonstrated a moderate scatter. However, these fits are relatively good given the long integration timescales and the chaos involved in the dynamics.

The distribution of the orbital elements of the resulting simulated stream are presented in Fig. 26. As in the previous cases, there was a substantial systematic offset between the simulated and the observed meteoroid geocentric speeds, orbital semi-major axes and eccentricity. We recall that, unlike the ARI, there are no optical detections of the DLTs, and hence no orbital elements for

comparison. However, apart from the poor fit in semi-major axis and eccentricity, the match in the angular orbital elements and the perihelion distance yield satisfactory results. Fig. 26 shows that the simulated width of the shower is somewhat wider compared to radar observations. The reason may be that within our simulations, we do not impose an activity level threshold, whereas in the case of CMOR a shower is defined by an activity level greater than 3σ above the median value of the sporadic background activity (see Section 2). The distributions of the orbital elements seem to change linearly during the activity period of the DLTs, and the simulated slope yields a good match to the observations.

4.1.6. Filament 3

Filament 3 (see Fig. 6) is located deep in the southern hemisphere with a mean sun-centered radiant location $(\lambda - \lambda_{\odot}) = 279.3^{\circ} \pm 3.1^{\circ}$ and $b = -63.3^{\circ} \pm 1.7^{\circ}$. Similar to previous filaments, a 3D wavelet search in the SAAMER database (Pokorný et al., 2017) indicated a radiant location resembling the θ -Carinids. The simulated activity profile of the shower is presented in Fig. 27 and compared to the SAAMER-derived profile. While the timing of the maximum activity was well reproduced, the overall width of the shower profile was not. The simulations predict an activity extending $272^{\circ} < \lambda_{\odot} < 283^{\circ}$ with the main peak activity at $\lambda_{\odot} = 276^{\circ}$ and a secondary maximum near $\lambda_{\odot} = 281^{\circ}$, the association of which with a separate shower is uncertain. However, we note that the available SAAMER observations span only 3 years and hence the shower might not be well defined due to small number statistics. Moreover, likely the shower is weak as well, as implied by the simulations (see Fig. 28). However, if the activity of the TCD is indeed only 5 days, that may well imply an extended activity of a few overlapping showers, a case similar to QUA and filament 1.

The best match between the predicted and observed activity profiles is obtained assuming initial meteoroid ejection onset from comet 96P circa 20000 BCE. However, that epoch is the furthest we went back in our backward simulations. In fact, the residuals of the profile fit did not converge and perhaps the TCDs may be older than 22,000 years. Fig. 28 shows that meteoroids ejected after 15000 BC would result in weak and scattered activity.

The simulated mean radiant location at $\lambda_{\odot} = 276^{\circ}$ is $\lambda - \lambda_{\odot} = 279.1^{\circ} \pm 3.0^{\circ}$ and $b = -61.6^{\circ} \pm 1.9^{\circ}$. That corresponds to a mean difference of 4° with the SAAMER-derived mean radiant (see Table 1 in Section 2 for comparison with SAAMER radiant), a difference also evident in the simulated radiant drift (Fig. 29). Interestingly, the simulated radiant drift shows a large scatter between individual meteoroids ($\Delta(\lambda - \lambda_{\odot}) \approx 15^{\circ}$), while SAAMER measures a drift of roughly 4° along the ecliptic and almost none in the ecliptic latitude. That large scatter may suggest that 96P contributes to other nearby shower/showers, though we did not find a candidate in the SAAMER database.

Furthermore, the shower consists mainly of old ejecta, a result that is also clear from Fig. 28. There is no obvious mass segregation along the radiant, though the stream seems to be dominated by relatively larger particles (millimeter size). Perhaps, similar to the QUA, there is a mechanism such as a mean-motion resonance with Jupiter which preferentially scatters away smaller particles or the action of PR drag has decreased the orbits of small particles, so that they do not presently intersect the Earth.

The fit to the observed distribution of the orbital elements of TCD is presented in Fig. 30. Our simulations predict systematically higher values of the orbital semi-major axis $a \approx 3$ AU, whereas SAAMER measures a mean value of about 2 AU. We note that we did not find optical observations of the TCD in the literature, so we can not determine the reliability of our estimations and the degree of discrepancy with optical surveys. The simulated orbital eccentricity is also somewhat higher, though within the measurement uncertainties. A close inspection of Fig. 30 reveals a

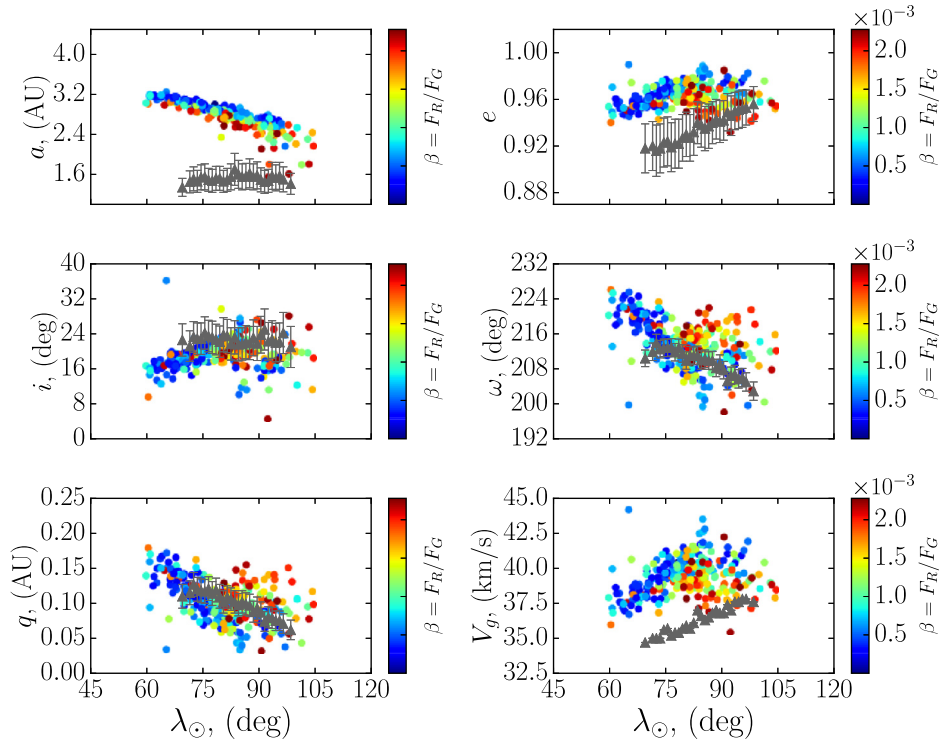


Fig. 26. Simulated distribution of the orbital elements of the filament 2 (color dots) for assumed meteoroid ejection onset epoch in 20000BCE from comet 96P. The color coding is in terms of meteoroids' β -parameter (equivalent to meteoroid size). Superimposed is the observed distributions by CMOR (black circles). (For interpretation of the references to color in this figure legend, the reader is referred to the web version of this article.)

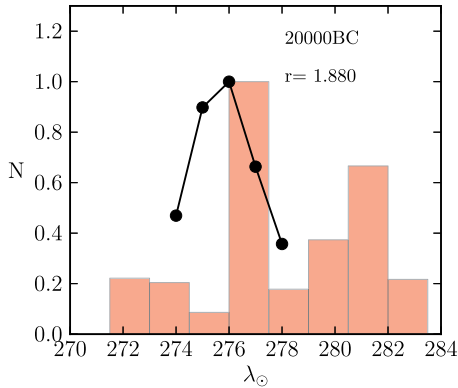


Fig. 27. Simulated, weighted and normalized activity profile of filament 3, originating from 96P/Machholz (red histogram) with meteoroid ejection onset in 20000BCE. The black circles corresponds to the observed normalized activity profile by SAAMER. (For interpretation of the references to color in this figure legend, the reader is referred to the web version of this article.)

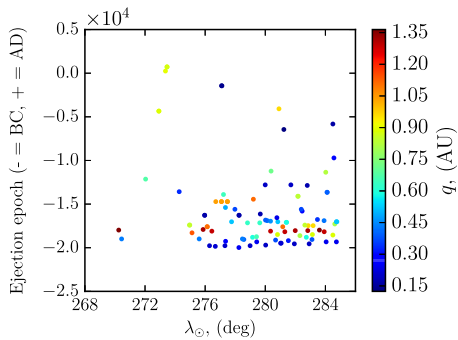


Fig. 28. Solar longitude distribution of filament 3 as a function of meteoroid ejection epoch, from comet 96P/Machholz. Individual meteoroids are color coded in terms of their perihelion distance at time of ejection. (For interpretation of the references to color in this figure legend, the reader is referred to the web version of this article.)

steep drop in all observed orbital elements except the inclination beyond $\lambda_{\odot} = 276^{\circ}$, which if real (not due to low meteor number statistics) suggests the existence of another nearby shower.

4.1.7. Filament 4

Filament 4, according to our simulations, corresponds to a meteor shower from a mean radiant position $(\lambda - \lambda_{\odot}) = 260.3^{\circ} \pm 2.8^{\circ}$ and $b = -62.6^{\circ} \pm 1.9^{\circ}$. A 3D wavelet search (see Section 2) in the SAAMER database indicated a radiant location resembling the KVE shower that is found the southern toroidal source. Fig. 31 shows the simulated and weighted activity profile of the KVE, compared to SAAMER observations. Interestingly, this activity range is similar to that of filament 3, that was identified as the TCD. In fact, both filaments seem to have approximately the same duration and peak at the same time (see Fig. 27 for comparison), though their mean radiant positions are separated by about 20° (see Table 1 in Section 2).

The best match between the theoretical and observed profiles is obtained assuming meteoroid ejection onset time circa 19000 BCE. The fit is relatively good, though the simulations predict a slightly longer activity of $\Delta\lambda_{\odot} \approx 4$ days. Our modelling did not yield a clear peak, though an average maximum seems to be found near $\lambda_{\odot} \approx 277^{\circ}$ or roughly 1 day later than the observed one. This small discrepancy may be due to uncertainties in our simulations or also may be indicate an older age. Generally, the orbital nodes regress over time for prograde orbits, so an older age may account for the difference in timing between the simulated and observed shower profile. However, the stream can not be younger than 20,000 years, as meteoroids ejected prior to 19000 BCE result in narrow profile and low activity, inconsistent with the observations (see on-line SM). Furthermore, as seen from Fig. 32, filament 4 seems to be mainly dominated by old ejecta. In fact, the bulk of the particles are released prior to 15000 BCE, with only a small fraction of recent ejecta (2000 BCE). Moreover, old particles released circa 13000 BCE and 17000 BCE, have been ejected from orbits of low

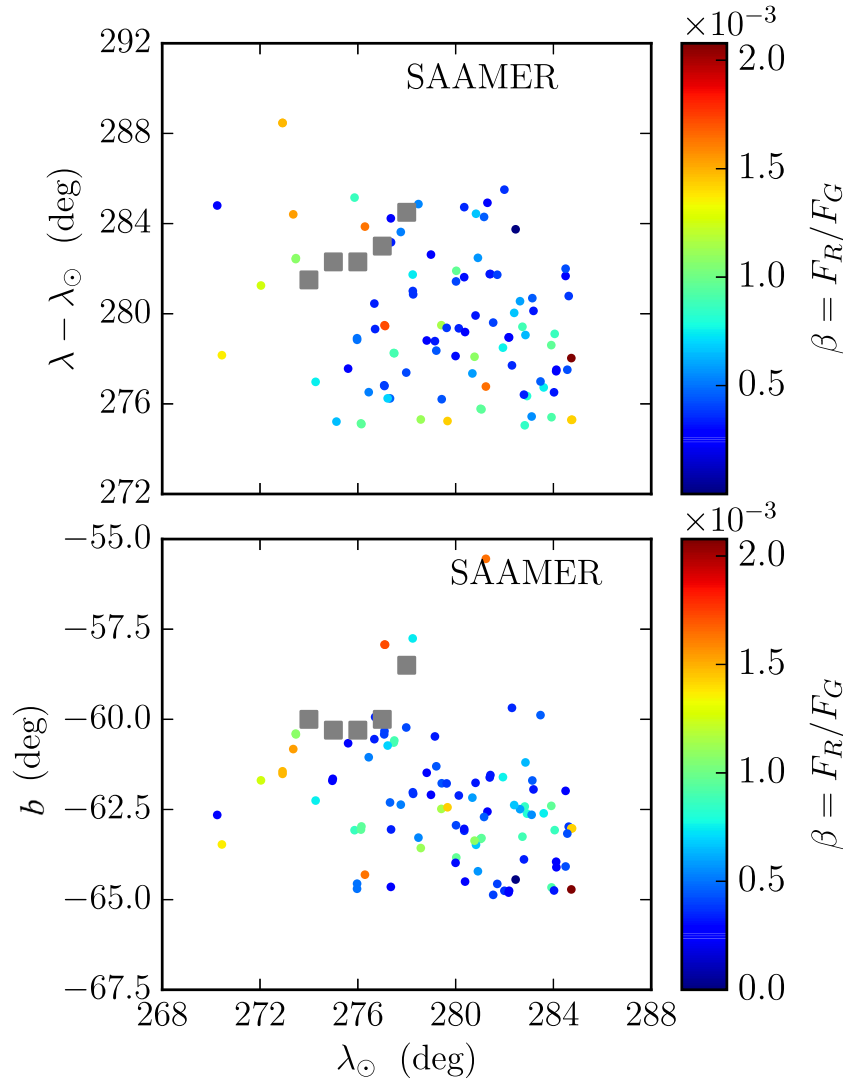


Fig. 29. Simulated sun-centered radiant drift of filament 3, with assumed meteoroid ejection onset in 20000 BCE from comet 96P. The color coding is in terms of meteoroid size. Superimposed is the observed radiant drift by SAAMER (grey squares). (For interpretation of the references to color in this figure legend, the reader is referred to the web version of this article.)

perihelion distance, so these particles are weighted more, which results in a relatively wide profile.

The simulated radiant drift (Fig. 33) results in a good fit to the SAAMER observations. However, as with previous showers, we do not observe a strong mass segregation along the radiant, though it is evident that the showers is mostly dominated by old ejecta and large particles.

Fig. 34 shows the simulated distribution of the orbital elements of the KVE, assuming meteoroid ejection onset time circa 19000 BCE. As with the previous showers, there is an obvious systematic shift in the predicted and measured geocentric speeds and thus the orbital semi-major axis and eccentricity, though the angular orbital elements produce a relatively good match. Also noteworthy is the systematic difference in the perihelion distance between the simulations and observations, a discrepancy also seen for filament 3 (TCD) in Section 4.1.6 and whose nature is not clearly understood.

4.2. The simulated meteor showers of parent candidate - P/1999 J6

In this section, we present our results of the meteoroid stream simulations associated with the Marsden group of comets, assuming that P/1999J6 can be taken as a representative parent

body for the group as a whole. Following the scenario suggested by Sekanina and Chodas (2005), wherein a single large comet broke up between 100 CE and 950 CE and formed the Marsden group of comets and the ARI, SDA, and NDA, we investigate the individual showers that comet P/1999J6 may produce during its secular evolution. The resulting simulated showers are presented in Fig. 35, where the individual showers are investigated below.

4.2.1. The Southern δ -Aquiriids

Fig. 36 shows the simulated activity profile of the SDAs, assuming a meteoroid ejection onset time circa 100 CE, from comet P/1999J6. The predicted pre-peak portion of the profile and the timing of the peak activity ($\lambda_{\odot} = 123.5$) produced a good fit to the observations, though the overall width was too narrow compared to radar and visual observations. It is evident from Fig. 38 that mostly particles ejected between 700 CE and 1500 CE dominate the peak of the SDAs. However, if the contribution of 96P, assuming meteoroid ejection onset in 17000 BCE, is added to the activity profile then the fit to the radar observation is significantly improved (see Fig. 37).

The simulated mean radiant location at $\lambda_{\odot} = 123.5^{\circ}$ was $\lambda - \lambda_{\odot} = 209.2^{\circ} \pm 0.4^{\circ}$ and $b = -4.8^{\circ} \pm 0.3^{\circ}$. Although the simulated radiant was very narrow, overall it was systematically shifted

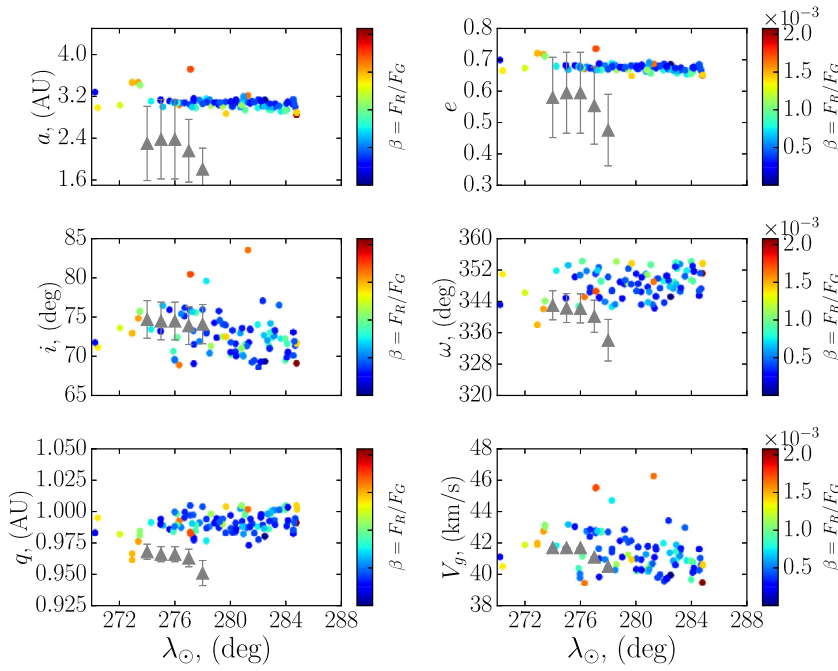


Fig. 30. Simulated distribution of the orbital elements of the filament 3 (color dots) for assumed meteoroid ejection onset epoch in 20000 BCE from comet 96P. The color coding is in terms of meteoroids' β -parameter (equivalent to meteoroid size). Superimposed is the observed distribution from SAAMER (grey triangles). (For interpretation of the references to color in this figure legend, the reader is referred to the web version of this article.)

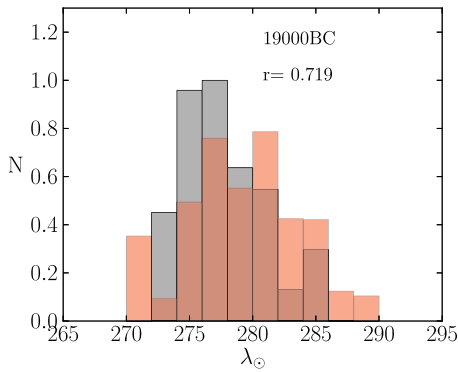


Fig. 31. Simulated, weighted and normalized activity profile (red histogram) of filament 4, originating from 96P/Machholz with meteoroid ejection onset in 19000 BCE. Superimposed are the observed normalized relative activity profiles by SAAMER (grey histogram). The quantity r denotes the sum of the residuals of the fit between the theoretical and SAAMER profile. (For interpretation of the references to color in this figure legend, the reader is referred to the web version of this article.)

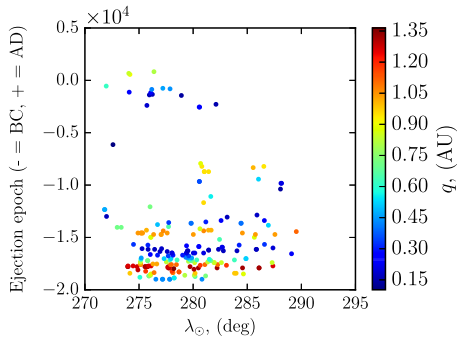


Fig. 32. Solar longitude distribution of filament 4 as a function of meteoroid ejection epoch, from comet 96P/Machholz. Individual meteoroids are color coded in terms of their perihelion distance at time of ejection. (For interpretation of the references to color in this figure legend, the reader is referred to the web version of this article.)

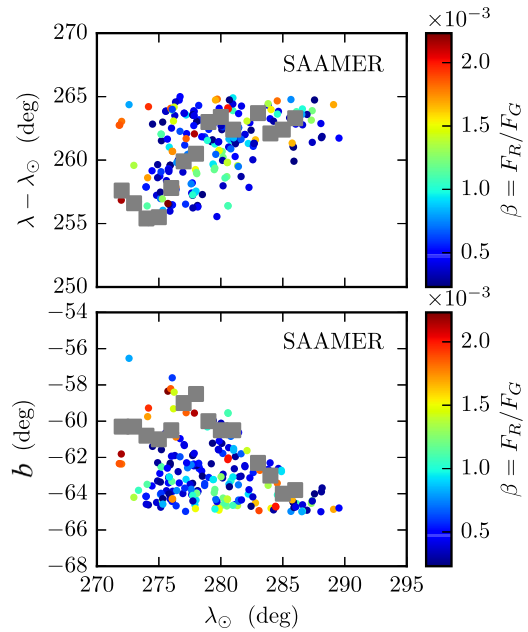


Fig. 33. Simulated sun-centered radiant drift of KVE, with assumed meteoroid ejection onset in 19000 BCE from comet 96P. The color coding is in terms of meteoroid size. Superimposed is the observed radiant drift by CMOR (grey squares). (For interpretation of the references to color in this figure legend, the reader is referred to the web version of this article.)

by 3.5° from the CMOR-derived mean radiant (see Table 1 in Section 2 for comparison). The simulated geocentric radiant drift of the SDA, originating from P/1999J6 only, is presented in Fig. 39. The fit to the observations was good before $\lambda_{\odot} = 125^\circ$, though beyond that point the simulated drift was higher than the measured one.

Fig. 40 shows the simulated distribution of the orbital elements of the SDA originating from comet P/1999J6, assuming meteoroid ejection onset time in 100 CE. As with previous showers, there

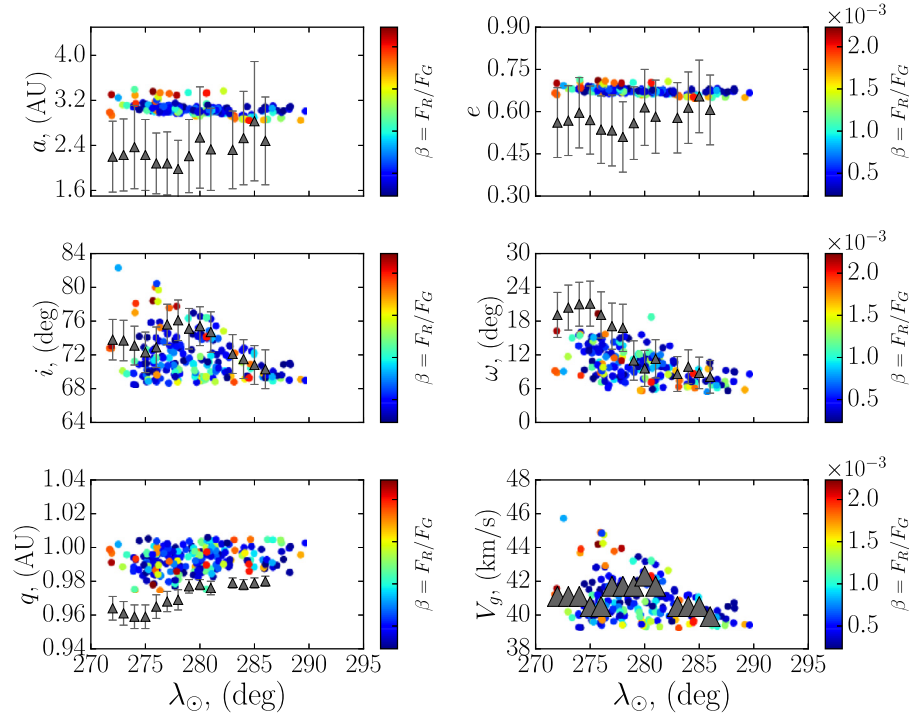


Fig. 34. Simulated distribution of the orbital elements of the KVE (color dots) for assumed meteoroid ejection onset epoch in 19000 BCE, from comet 96P. The color coding is in terms of meteoroids' β -parameter (equivalent to meteoroid size). Superimposed are the observed distributions SAAMER (black circles). (For interpretation of the references to color in this figure legend, the reader is referred to the web version of this article.)

was a systematic difference between the theoretical and the radar-derived geocentric speeds of the meteoroids, resulting in systematic discrepancy in the semi-major axis. More specifically, in the range $115^\circ < \lambda_\odot < 125^\circ$, where the best match between our simulated and the observed activity profile was observed, our predicted meteoroids' geocentric speeds were overestimated by $\Delta V_g \approx 1.5 \text{ km s}^{-1}$ compared to both CMOR and CAMS. However, the theoretical values of the meteoroids' semi-major axis were within the statistical uncertainty of the values measured by CAMS, though CMOR's values were underestimated by approximately 1 AU.

Finally, considering the fit of our simulated activity profile to the observed one, the origin of the SDA as being solely due to ejections from P/1999 J6, between 100 CE and 950 CE is not supported by our simulations. The resulting shower duration from P/1999 J6 is too short. Hence, we conclude the Marsden group of comets can not alone reproduce the observed profile features of the SDAs. The longer activity of the shower requires inclusion of older particles, consistent with much of the dust being related to 96P. In fact, the most plausible scenario, according to our simulations, is that comet 96P was captured into a short period orbit circa 17000 BCE, and suffered a major breakup in 100 CE, which resulted in the formation of the Marsden group of comets. Comet 96P is the dominant parent of the SDAs, where the Marsden group of comets contribute mainly to the pre- peak portion of the stream.

4.2.2. Filament 1 and 3

According to our simulations, there is a negligible contribution by P/1999 J6 to filament 1 and filament 3, in the northern and southern toroidal sources respectively. Using a 3D wavelet search, filament 1 seems to resemble the NID or DADs as described in Section 4.1.4. In contrast, the radiant location of filament 3 was in the proximity of the TCD (see Section 4.1.6). We omit the visual representation of these filaments here due to their low number of particles in each of these radiants. The radiant of filament 1 consists of 2 particles, whereas 5 meteoroids contribute to filament 3.

Perhaps, if our initial meteoroid ejection was earlier than 100 AD, the abundance of the particles in those filaments would be higher but we did not investigate this.

4.2.3. Filament 4

Our numerical simulations indicate that comet P/1999 J6 contributes to the KVE (filament 4 from Section 4.1.7). The simulated activity profile is presented in Fig. 41. Similar to the SDA, the timing of the shower is reproduced well, while the overall width of the profile is not. The resulting FWHM of the profile corresponds to approximately 2 days, whereas SAAMER measures FWHM $\approx 10^\circ$. The bulk of the meteoroids are old, in the sense they have been ejected between 100 CE and 1000 CE, but they did not have enough time to spread across the width of the stream (see Fig. 43). It is also evident that meteoroids released after 1000 CE do not presently reach the Earth.

Clearly, there is a need for an older meteoroid supply or for an additional parent. In Section 4.1.7 we showed that most of the observed characteristics of the KVE can be explained by a meteoroid ejection onset time from 96P after 19000 BCE. Indeed, if the latter contribution is added, the overall simulated activity profile produces a better fit to the observations (see Fig. 42). Thus, the observed activity profile is consistent with a capture of 96P into a short period orbit circa 20000 BCE, followed by a major fragmentation of the comet near 100 CE, resulting in the formation of the Marsden group of comets. The subsequent independent evolution of the Marsden group of comets supplied meteoroids mainly to the core of the KVE. We recall that a similar scenario was proposed by Sekanina and Chodas (2005), except that observed features of the activity profile of the KVE can not be explained by cometary activity of the Marsden group of comets alone over only 2000 years.

The simulated sun-centered radiant (Fig. 44) drift yields a poor match to the SAAMER observations. The latter measures only a moderate drift, while the simulations predict a large motion in each dimension, $(\lambda - \lambda_\odot)$ and b , in the range of the simulated

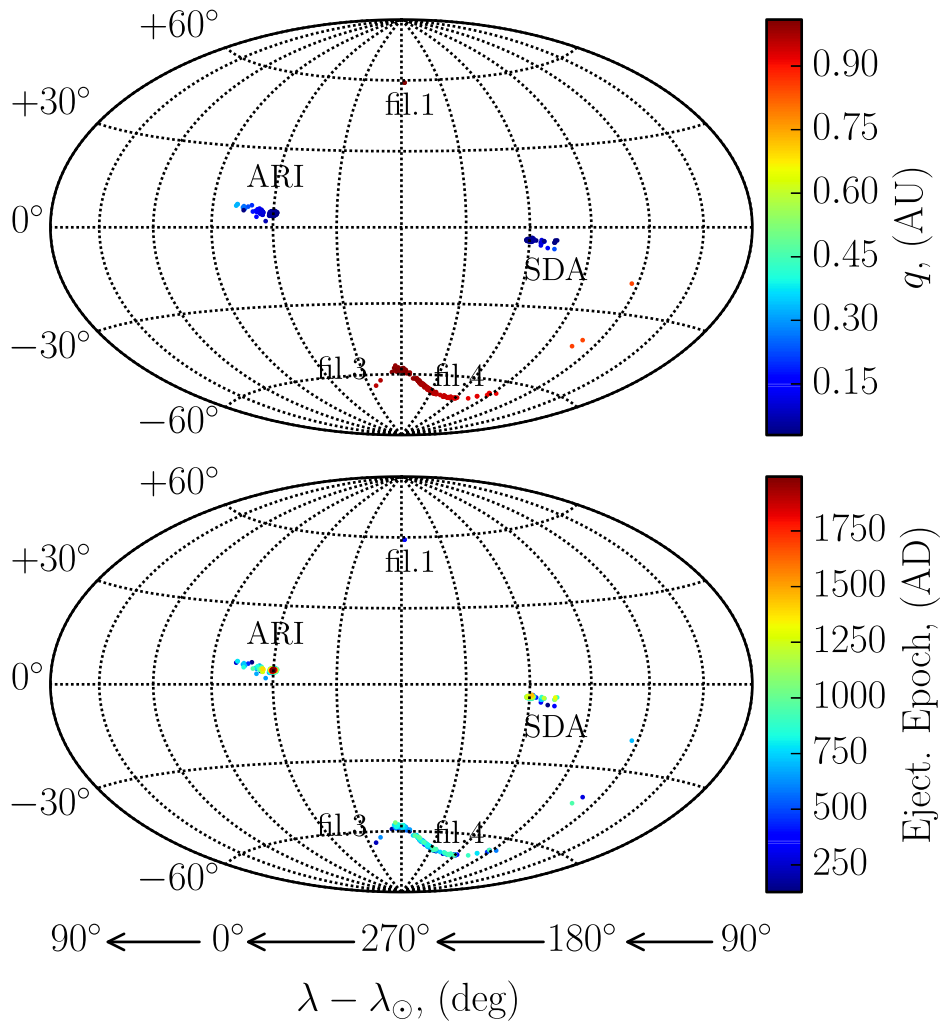


Fig. 35. Resulting radiant distribution of meteoroids ejected from a single clone of comet P/1999 J6 with meteoroid ejection onset time 100 CE. The radiants in top panel are color coded in terms of meteoroids' present perihelion distance, and as a function of meteoroid ejection speed (lower panel). (For interpretation of the references to color in this figure legend, the reader is referred to the web version of this article.)

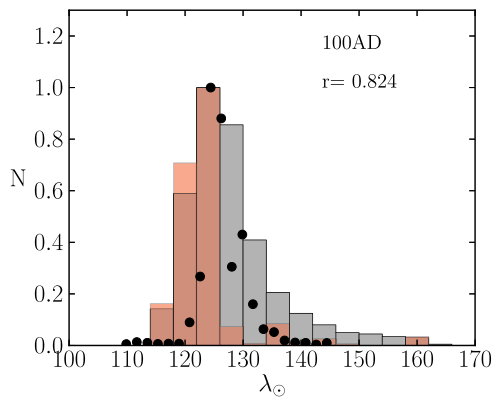


Fig. 36. Simulated, weighted and normalized activity profile (red histogram) of the SDA, originating from comet P/1999 J6 with meteoroid ejection onset in 100 CE. Superimposed are the observed normalized relative activity profiles by CMOR (grey histogram) and IMO visual observations (black circles). The quantity r denotes the sum of the residuals of the fit between the theoretical and CMOR profile. (For interpretation of the references to color in this figure legend, the reader is referred to the web version of this article.)

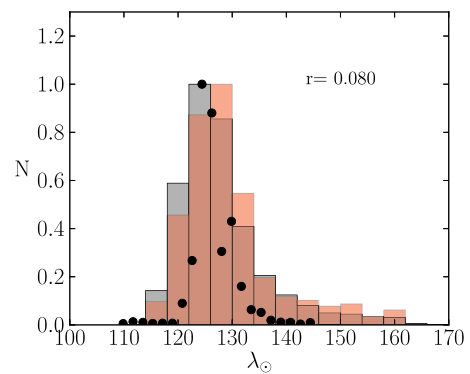


Fig. 37. The combined simulated activity profile of the SDA (red histogram), assuming meteoroid contribution from both, 96P and P/1999 J6. The assumed meteoroid ejection onset of 96P/Machholz is 17000 BCE, and meteoroid ejection onset of P/1999 J6 in 100 CE. The grey histogram corresponds to the observed activity profile by CMOR, while the circles are activity measured from visual observations of the IMO. (For interpretation of the references to color in this figure legend, the reader is referred to the web version of this article.)

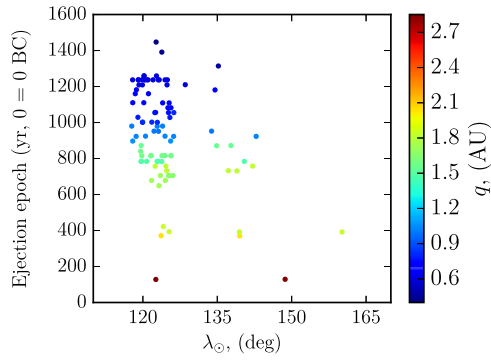


Fig. 38. Solar longitude distribution of SDA as a function of meteoroid ejection epoch, from comet P/1999J6. Individual meteoroids are color coded in terms of their perihelion distance at time of ejection. (For interpretation of the references to color in this figure legend, the reader is referred to the web version of this article.)

activity. Since, both the predicted and measured drifts intersect, they are only consistent over a short time, corresponding to the narrow peak of the activity profile. That clearly indicates that the Marsden group of comets are not the sole parent of the shower, where our simulations show that the dominant contributor to the shower is comet 96P (see Section 4.1.7).

Fig. 45 shows the predicted distribution of the orbital elements of the KVE across the simulated activity period. Apart from the poor fit to the measured semi-major axis and eccentricity, the simulated angular orbital elements seem to be consistent with observations within a narrow time interval, corresponding to the predicted activity period of the shower resulting from P/1999J6. An interesting feature is that the simulated orbital elements split into two groups, a difference that is most noticeable in the (i, λ_{\odot}) , $(\omega, \lambda_{\odot})$, (q, λ_{\odot}) and (V_g, λ_{\odot}) space. The simulations predict meteoroids with orbits that span a wide range of orbital element values within a few days, a feature not supported by the SAAMER observations. The measured orbital elements by SAAMER do predict a drift as a function of the solar longitude, though moderate

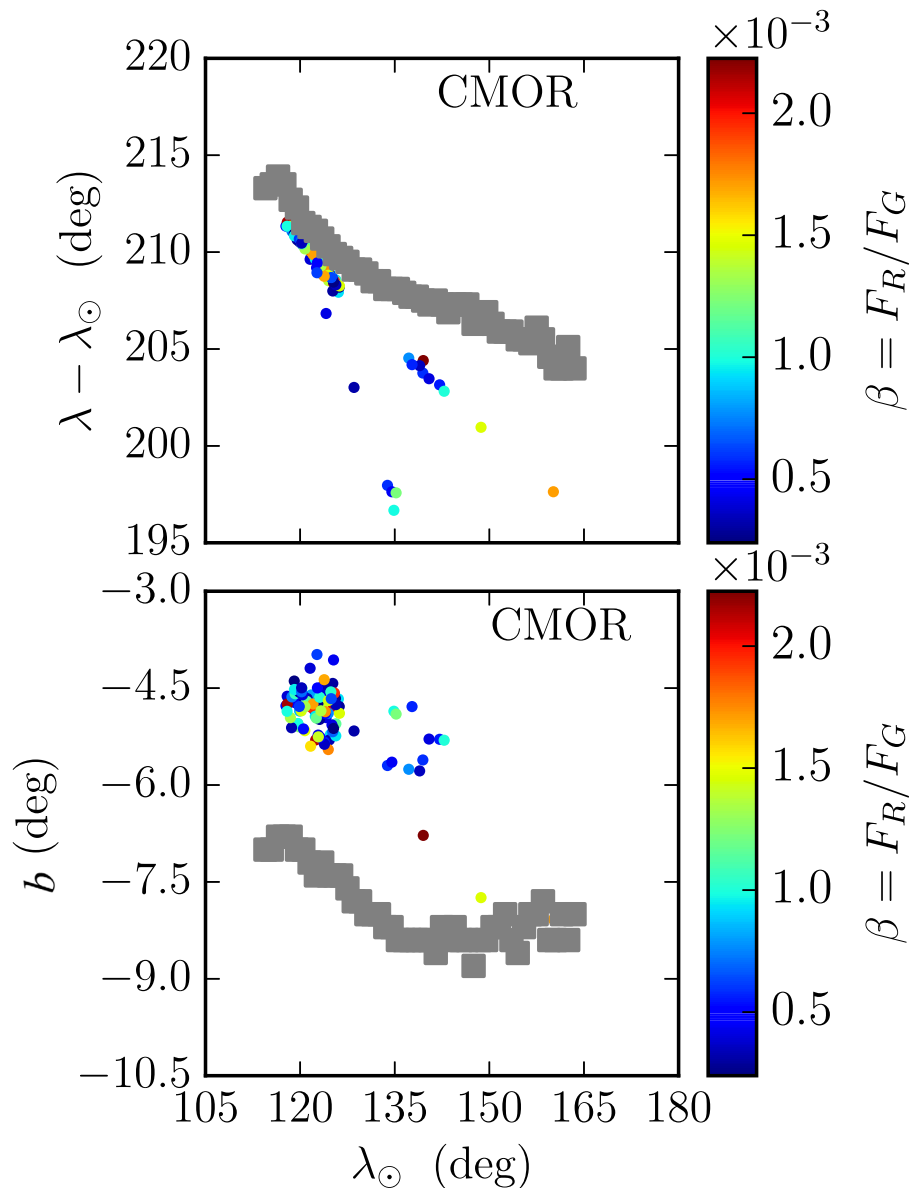


Fig. 39. Simulated sun-centered radiant drift of SDA, with assumed meteoroid ejection onset in 100CE from comet P/1999J6. The color coding is in terms of meteoroid size. Superimposed is the observed radiant drift by CMOR (grey squares). (For interpretation of the references to color in this figure legend, the reader is referred to the web version of this article.)

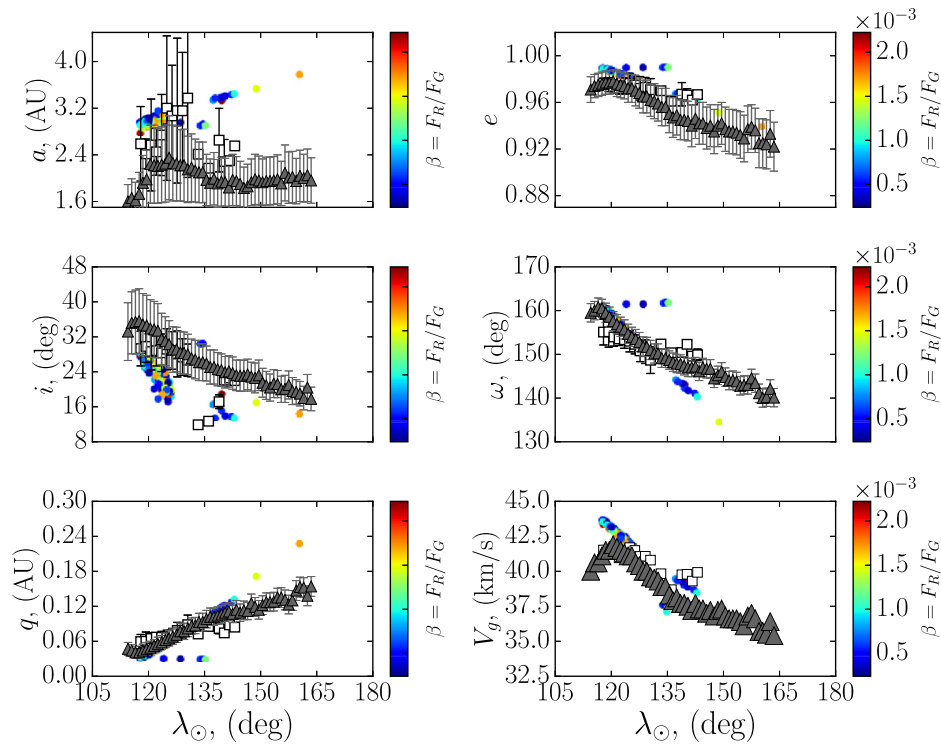


Fig. 40. Simulated distribution of the orbital elements of the SDA (color dots) for assumed meteoroid ejection onset epoch in 100 CE from comet P/1999J6. The color coding is in terms of meteoroids' β -parameter (or equivalent to meteoroid size). Superimposed are the observed distributions by CAMS (open squares) and CMOR (grey triangles). (For interpretation of the references to color in this figure legend, the reader is referred to the web version of this article.)

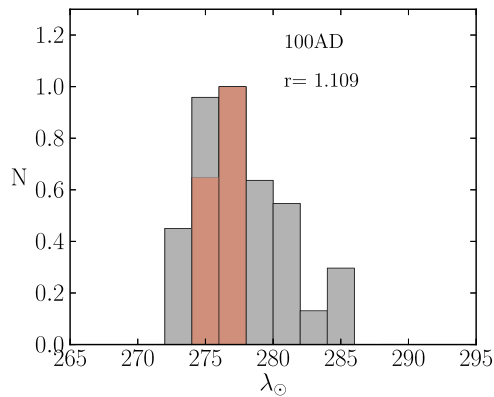


Fig. 41. Simulated, weighted and normalized activity profile (red histogram) of filament 4, originating from comet P/1999J6 with meteoroid ejection onset in 100 CE. Superimposed is the observed normalized relative activity profiles by SAAMER (grey histogram). The quantity r denotes the sum of the residuals of the fit between the theoretical and SAAMER profile. (For interpretation of the references to color in this figure legend, the reader is referred to the web version of this article.)

and more gradual. Due to the poor match of the simulations to the observed shower characteristics of the KVE, the Marsden group of sunskirters does not seem to be the dominant parent of the shower, but may contribute to the core of stream.

5. Discussion and conclusions

We performed numerical simulations to investigate the individual meteoroid streams of comets 96P/Machholz and the most prominent member of the Marsden group of comets, P/1999 J6. Our goal was to obtain a self-consistent scenario of the past dynamical evolution of the interplanetary bodies associated with comet 96P, and to determine the parent producing most of the meteoroids from the associated streams now visible at the Earth.

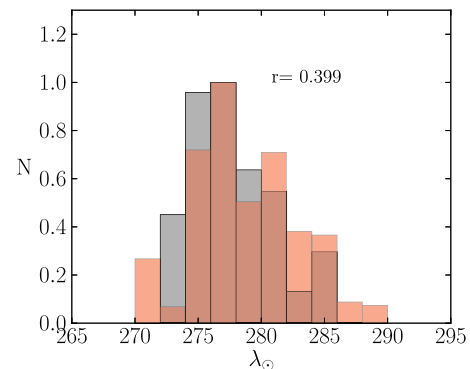


Fig. 42. The combined simulated activity profile of the filament 4 (red histogram). The assumed meteoroid ejection onset of 96P/Machholz is 20000 BCE, and meteoroid ejection onset of P/1999 J6 in 100 CE. The grey histogram corresponds to the activity profile as measured by SAAMER. The number " r " is sum of the residuals from the fit. (For interpretation of the references to color in this figure legend, the reader is referred to the web version of this article.)

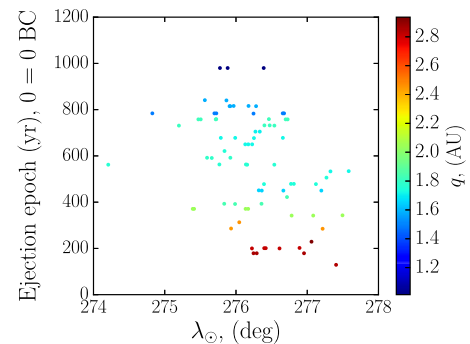


Fig. 43. Solar longitude distribution of filament 4 as a function of meteoroid ejection epoch, from comet P/1999J6. Individual meteoroids are color coded in terms of their perihelion distance at time of ejection. (For interpretation of the references to color in this figure legend, the reader is referred to the web version of this article.)

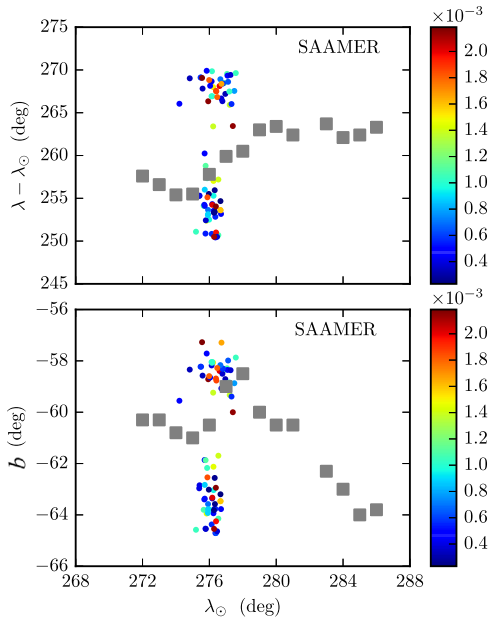


Fig. 44. Simulated sun-centered radiant drift of KVE, with assumed meteoroid ejection onset in 100 CE from comet P/1999 J6. The color coding is in terms of meteoroid size. Superimposed is the observed radiant drift by CMOR (grey squares). (For interpretation of the references to color in this figure legend, the reader is referred to the web version of this article.)

In addition, we also aimed to establish a possible past fragmentation chronology of a single large first precursor, presumably giving rise to the Marsden group of sunskirting comets (Sekanina and Chodas, 2005). The relative contribution of each parent to the complex is determined, by simultaneous matching and investigation of the observed characteristics of their resulting showers. As

observational shower constraints we used radar, optical and visual activity measurements from CMOR, SAAMER, CAMS and IMO.

Our simulations confirm the results of Babadzhanov and Oubrov (1992) and Neslušan et al. (2013b) that within one full Kozai circulation cycle, the ascending and descending nodes of comet 96P intersect the Earth’s orbit in eight different locations, and thus result in eight different meteor showers. Four of these showers are found in the ecliptic sporadic meteoroid sources and four belong to the Northern and Southern toroidal sources, respectively. Furthermore, four of these showers are well known, the Quadrantids (QUA), the daytime Arietids (ARI), the Southern and Northern δ -Aquiriids (SDA and NDA), whereas the remaining four showers are weak and have less well determined characteristics. We call these weak showers “filaments”:

Filament 1, which was previously identified by Babadzhanov and Oubrov (1992) as the Ursids, is found in the north toroidal source and is likely associated with the “November ι -Draconids (NID)” or with the “December α -Draconids (DAD)”. The two showers peak at the same time and have radiants partially overlapping, so their separation as individual showers was not possible in this work, a result initially suggested by Neslušan et al. (2013b). Filament 2 resembles the “daytime λ -Taurids (DLT)” and appears to be consistent with the long-sought southern branch of the daytime Arietids. Filament 3 and 4 likely correspond to the θ -Carinids (TCD) and κ -Velids (KVE) respectively, found in the southern toroidal source. Similar to filament 1, the TCD and KVE appear to peak at the same time, though their radiant locations are separated by 20°. However, the separation of filaments 3 and 4 is more obvious and they appear to be two distinct showers. We note that the DLT, TCD and the DAD (or NID) were identified by Babadzhanov and Oubrov (1992) as the α -Cetids, Carinids and Ursids, respectively. Among these showers, the most active are the QUA, followed in order of apparent strength by the ARI, SDA, NDA, DLT, KVE, NID or DAD and the TCD.

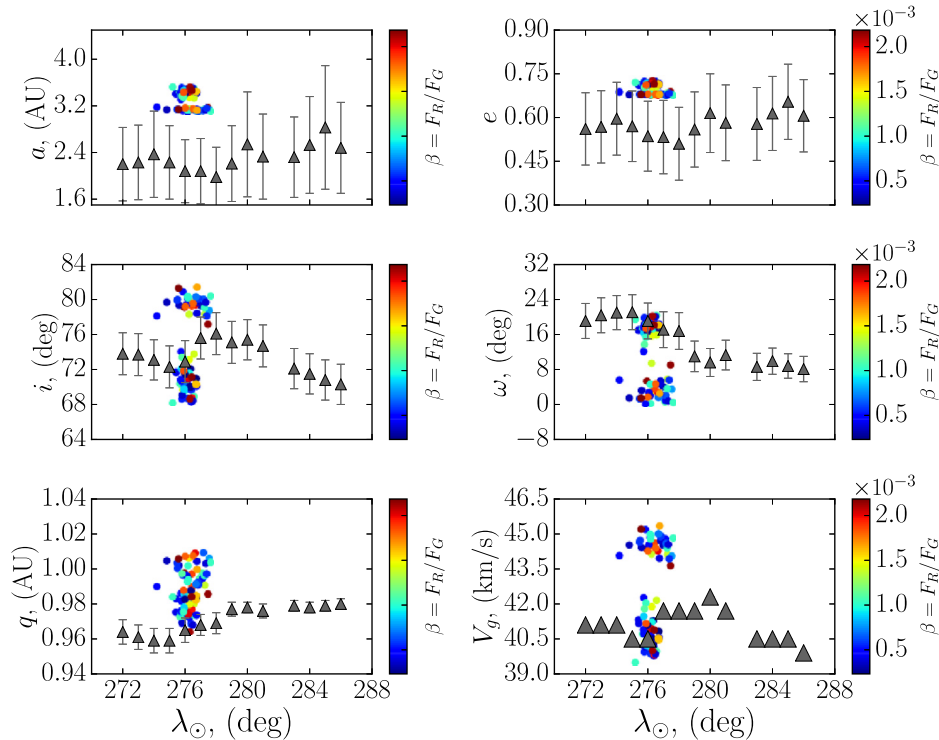


Fig. 45. Simulated distribution of the orbital elements of the KVE (color dots) for assumed meteoroid ejection epoch in 100 CE from comet P/1999 J6. The color coding is in terms of meteoroids’ β -parameter (equivalent to meteoroid size). Superimposed is the observed distributions by SAAMER (black circles). (For interpretation of the references to color in this figure legend, the reader is referred to the web version of this article.)

We use the width of the wings and shape of the observed activity profile as a strong proxy as to the age of individual showers to fit to our simulated meteoroid streams. We find that ages of the eight showers, assumed to originate solely from 96P, range between 10000 BCE and 20000 BCE.

The best match between the duration of the simulated and observed activity profiles for the QUA is obtained assuming an initial meteoroid ejection onset from 96P in 10000 BCE. We did not attempt to match the narrow or core portion of the shower, which we showed in a previous work (Abedin et al., 2015) to be associated with asteroid 2003 EH₁.

The simulated width of the ARI requires a meteoroid ejection onset time at least 12,000 years ago (Abedin et al., 2017), whereas the bulk of the activity profile of the SDA can be reproduced assuming that 96P was captured in a short period orbit circa 17000 BCE. A similar result is obtained for the NDA, with a best fit between the simulated and observed duration of the shower for meteoroid ejection onset in 17000 BCE. The observed widths of the profiles of filament 1, 2, 3 and 4 can only be explained if the comet became active circa 19000 BCE.

Assuming the scenario proposed by Sekanina and Chodas (2005) for the formation of the Marsden group of comets and the ARI, SDA and NDA in a major comet break-up event between 100 CE and 950 CE, we simulated the possible showers associated with comet P/1999J₆, taking this to be a substitute for the Marsden group of comets as a whole. Our simulations confirm that the Marsden group of comets contribute to the ARI, SDA and three weak filaments (filament 1, 3 and 4 associated with 96P), though we find that P/1999J₆ is not the parent of the NDA, in contradiction to previous suggestions (Ohtsuka et al., 2003; Sekanina and Chodas, 2005; Jenniskens, 2006). Furthermore, using a 3D wavelet search in the CMOR and SAAMER database, the three weak filaments are identified as part of the NID or DAD, the TCD and KVE showers, respectively. However, the contribution of the comet to filaments 1 and 3 is extremely low, with only a few particles in our simulations approaching the Earth. Finally, assuming even the earliest fragmentation epoch, 100 CE, suggested by Sekanina and Chodas (2005), our simulations indicate the Marsden group of comets can not alone explain the observed wide activity profiles of the showers associated with it (ARI, SDA, NDA, KVE, TCD and NID or DAD). There is a need for meteoroid ejection over at least a few tens of millennia in order for the observed width of the activity profiles to be explained.

In summary, the bulk of the observed characteristics of the meteor showers associated with comet 96P can be explained if the comet was captured into a short period orbit circa 20000 BCE and has been active until the present. Then there is sufficient time for it to produce most of the features the QUA, ARI, SDA, NDA, DLT, KVE, TCD and the NID or DAD. However, a better match to the activity profiles is produced if we also add the scenario by Sekanina and Chodas (2005), namely the break-up of 96P after 100 CE, which formed the Marsden group of comets, and perhaps other sungrazing comets. The meteoroid supply from the Marsden group of comets complement the observed features of these showers, though mainly contribute to their peak activity.

Acknowledgments

Funding for this research was provided by the Canada Research Chair program, the Natural Sciences and Engineering Research Council of Canada (NSERC) and NASA co-operative agreement NNX15AC94A.

The deployment of SAAMER and its remote receiving stations was supported by NSF awards AGS-0634650, AGS-0944104, and AST-0908118 and currently by the NASA-Solar System Observation Program. DJ's participation is currently supported through

NASA awards 12-PAST12-0007 and 12-PATM12-0006 and SSO. The authors wish to give special thanks to the EARG personnel for their invaluable assistance with the operation and day-to-day oversight of SAAMER. Without their help, operating a system on the other side of the planet would be impossible!

References

- Abedin, A., Spurný, P., Wiegert, P., Pokorný, P., Borovička, J., Brown, P., 2015. On the age and formation mechanism of the core of the quadrantid meteoroid stream. *Icarus* 261, 100–117. [arXiv:1508.02418](https://arxiv.org/abs/1508.02418).
- Abedin, A., Wiegert, P., Pokorný, P., Brown, P., 2017. The age and the probable parent body of the daytime arietid meteor shower. *Icarus* 281, 417–443.
- A'Hearn, M.F., Millis, R.C., Schleicher, D.O., Osip, D.J., Birch, P.V., 1995. The ensemble properties of comets: results from narrowband photometry of 85 comets, 1976–1992. *Icarus* 118, 223–270.
- Babadzhanov, P.B., Obrubov, Y.V., 1992. P/machholz 1986 8 and quadrantid meteoroid stream. orbital evolution and relationship. In: Harris, A., Bowell, E. (Eds.), *Asteroids, Comets, Meteors 1991*, pp. 27–32.
- Babadzhanov, P.B., Williams, I.P., Kokhirova, G.I., 2008. Meteor showers associated with 2003eh1. *MNRAS* 386, 2271. [/doi/10.1111/j.1365-2966.2008.13202.x](https://doi.org/10.1111/j.1365-2966.2008.13202.x) [/journal/mnras/386/4/10.1111/j.1365-2966.2008.13202.x](https://onlinelibrary.wiley.com/doi/10.1111/j.1365-2966.2008.13202.x) [/2/mnras0386-2271.pdf](https://onlinelibrary.wiley.com/doi/10.1111/j.1365-2966.2008.13202.x)
- Bailey, M.E., Chambers, J.E., Hahn, G., 1992. Origin of sungrazers - a frequent cometary end-state. *A & A* 257, 315–322.
- Brown, P., Jones, J., 1998. Simulation of the formation and evolution of the perseid meteoroid stream. *Icarus* 133, 36–68.
- Brown, P., Weryk, R.J., Wong, D.K., Jones, J., 2008. A meteoroid stream survey using the canadian meteor orbit radar. i. Methodology and radiant catalogue. *Icarus* 195, 317–339.
- Brown, P., Wong, D.K., Weryk, R.J., Wiegert, P., 2010. A meteoroid stream survey using the canadian meteor orbit radar. II: Identification of minor showers using a 3d wavelet transform. *Icarus* 207, 66–81.
- Bruzzone, J.S., Brown, P., Weryk, R.J., Campbell-Brown, M.D., 2015. A decadal survey of the daytime arietid meteor shower using the canadian meteor orbit radar. *MNRAS* 446, 1625–1640.
- Burns, J.A., Lamy, P.L., Soter, S., 1979. Radiation forces on small particles in the solar system. *Icarus* 40, 1–48.
- Campbell-Brown, M., Brown, P.G., 2015. A 13-year radar study of the η -aquariid meteor shower. *MNRAS* 446, 3669–3675.
- Chambers, J.E., 1999. A hybrid symplectic integrator that permits close encounters between massive bodies. *MNRAS* 304, 793–799.
- Delsemme, A.H., 1982. Chemical composition of cometary nuclei. In: Wilkening, L. (Ed.), *IAU Colloq. 61: Comet Discoveries, Statistics, and Observational Selection*, pp. 85–130.
- Froeschle, C., Scholl, H., 1986. Gravitational splitting of quadrantid-like meteor streams in resonance with jupiter. *A&A* 158, 259–265.
- Goncz, R., Rickman, H., Froeschle, C., 1992. The connection between comet p/machholz and the quadrantid meteor. *MNRAS* 254, 627–634.
- Green, D.W.E., Rickman, H., Porter, A.C., Meech, K.J., 1990. The strange periodic comet machholz. *Science* 247, 1063–1067.
- Grun, E., Zook, H.A., Fechtig, H., Giese, R.H., 1985. Collisional balance of the meteoritic complex. *Icarus* 62, 244–272.
- Hasegawa, I., 1979. Orbits of ancient and medieval comets. *Publ. Astr. Soc. Japan* 31, 257–270.
- Hughes, D.W., Williams, I.P., Fox, K., 1981. The mass segregation and nodal retrogression of the quadrantid meteor stream. *MNRAS* 195, 625–637.
- Janches, D., Close, S., Hormaechea, J.L., Swarnalingam, N., Murphy, A., O'Connor, D., Vandepier, B., Fuller, B., Fritts, D.C., Brunini, C., 2015. The southern argentina agile METeor radar orbital system (SAAMER-OS): an initial sporadic meteoroid orbital survey in the southern sky. *ApJ* 809, 36.
- Janches, D., Hormaechea, J.L., Brunini, C., Hocking, W., Fritts, D.C., 2013. An initial meteoroid stream survey in the southern hemisphere using the southern argentina agile meteor radar (SAAMER). *Icarus* 223, 677–683.
- Jenniskens, P., 2004. 2003 EH₁ is the quadrantid shower parent comet. *Astron. J.* 127, 3018–3022.
- Jenniskens, P., 2006. Meteor showers and their parent comets.
- Jenniskens, P., Betlem, H., de Lignie, M., Langbroek, M., van Vliet, M., 1997. Meteor stream activity. v. The quadrantids, a very young stream. *A&A* 327, 1242–1252.
- Jenniskens, P., Duckworth, H., Grigsby, B., 2012. Daytime arietids and marsden sunskirters (ARI, IAU #171). *WGN, J. Int. Meteor Org.* 40, 98–100.
- Jenniskens, P., Lyytinen, E., de Lignie, M.C., Johannink, C., Jobse, K., Schievink, R., Langbroek, M., Koop, M., Gural, P., Wilson, M.A., Yrjölä, I., Suzuki, K., Ogawa, H., de Groot, P., 2002. Dust trails of 8p/tuttle and the unusual outbursts of the ursid shower. *Icarus* 159, 197–209.
- Jenniskens, P., Nénon, Q., Albers, J., Gural, P.S., Haberman, B., Holman, D., Morales, R., Grigsby, B.J., Samuels, D., Johannink, C., 2016. The established meteor showers as observed by CAMS. *Icarus* 266, 331–354.
- Jones, J., 2002. A model of the sporadic meteoroid complex. Technical report. The University of Western Ontario and NASA (MSFC).
- Jones, J., Jones, W., 1993. Comet machholz and the quadrantid meteor stream. *MNRAS* 261, 605–611.
- Joep, T.J., Williams, I.P., 2013. Stream and sporadic meteoroids associated with near-earth objects. *MNRAS* 430, 2377–2389.

- Kinoshita, H., Nakai, H., 1999. Analytical solution of the kozai resonance and its application. *Celest. Mech. Dyn. Astron.* 75, 125–147.
- Klačka, J., 2004. Electromagnetic radiation and motion of a particle. *Celest. Mech. Dyn. Astron.* 89, 1–61. arXiv:astro-ph/0301138.
- Klačka, J., Kocifaj, M., 2008. Times of inspiralling for interplanetary dust grains. *MNRAS* 390, 1491–1495.
- Kozai, Y., 1962. Secular perturbations of asteroids with high inclination and eccentricity. *Astron. J.* 67, 591.
- Kronk, G.W., 1999. *Cometography*, 1. Cambridge University Press, Cambridge.
- Lamy, P., Faury, G., Llebaria, A., Knight, M.M., A'Hearn, M.F., Battams, K., 2013. Sunskirting comets discovered with the LASCO coronagraphs over the decade 1996–2008. *Icarus* 226, 1350–1398.
- Lamy, P. L., Toth, I., Fernandez, Y. R., Weaver, H. A., 2004. The sizes, shapes, albedos, and colors of cometary nuclei. 223–264.
- Leinert, C., Grun, E., 1990. Interplanetary dust. 207.
- Levison, H.F., Duncan, M.J., 1994. The long-term dynamical behavior of short-period comets. *Icarus* 108, 18–36.
- Levison, H.F., Duncan, M.J., 1997. From the kuiper belt to jupiter-family comets: the spatial distribution of ecliptic comets. *Icarus* 127, 13–32.
- Licandro, J., Tancredi, G., Lindgren, M., Rickman, H., Hutton, R.G., 2000. CCD photometry of cometary nuclei, i: Observations from 1990–1995. *Icarus* 147, 161–179.
- McIntosh, B.A., 1990. Comet p/machholz and the quadrantid meteor stream. *Icarus* 86, 299–304.
- Neslušan, L., Hajduková, M., Jakubík, M., 2013. Meteor-shower complex of asteroid 2003 EH1 compared with that of comet 96p/machholz. *A&A* 560, A47.
- Neslušan, L., Kaňuchová, Z., Tomko, D., 2013. The meteor-shower complex of 96p/machholz revisited. *A&A* 551, A87.
- Ohtsuka, K., Nakano, S., Yoshikawa, M., 2003. On the association among periodic comet 96p/machholz, arietids, the marsden comet group, and the kracht comet group. *Publ. Astr. Soc. Jpn.* 55, 321–324.
- Pokorný, P., Janches, D., Brown, P.G., Hormaechea, J.L., 2017. An orbital meteoroid stream survey using the southern argentina agile MEteor radar (SAAMER) based on a wavelet approach. *Icarus* 290, 162–182.
- Schleicher, D.G., 2008. The extremely anomalous molecular abundances of comet 96p/machholz 1 from narrowband photometry. *Astron. J.* 136, 2204–2213.
- Schulz, R., 2006. Compositional coma investigations: gas and dust production rates in comets. In: Daniela, L., Sylvio Ferraz, M., Angel, F. (Eds.), *Asteroids, Comets, Meteors*, pp. 413–423.
- Sekanina, Z., 1988. Outgassing asymmetry of periodic comet encke. i - apparitions 1924–1984. *Astron. J.* 95, 911–924.
- Sekanina, Z., 1990. Periodic comet machholz and its idiosyncrasies. *Astron. J.* 99, 1268–1277.
- Sekanina, Z., 1992. Sublimation rates of carbon monoxide and carbon dioxide from comets at large heliocentric distances. In: Harris, A., Bowell, E. (Eds.), *Asteroids, Comets, Meteors 1991*.
- Sekanina, Z., Chodas, P.W., 2005. Origin of the marsden and kracht groups of sunskirting comets. i. Association with comet 96p/machholz and its interplanetary complex. *ApJS* 161, 551–586.
- SonotaCo, 2009. A meteor shower catalog based on video observations in 2007–2008. *WGN, J. Int. Meteor. Org.* 37, 55–62.
- Weryk, R.J., Brown, P.G., 2013. Simultaneous radar and video meteors-II: Photometry and ionisation. *Planet. Space Sci.* 81, 32–47.
- Whipple, F.L., 1950. A comet model. i. the acceleration of comet encke. *ApJ* 111, 375–394.
- Whipple, F.L., 1951. A comet model. II. physical relations for comets and meteors. *ApJ* 113, 464.
- Whipple, F.L., 1967. On maintaining the meteoritic complex. *NASA Spec. Pub.* 150, 409.
- Wiegert, P., Brown, P., 2005. The quadrantid meteoroid complex. *Icarus* 179, 139–157.
- Wiegert, P., Vaubaillon, J., Campbell-Brown, M., 2009. A dynamical model of the sporadic meteoroid complex. *Icarus* 201, 295–310.
- Williams, I.P., Collander-Brown, S.J., 1998. The parent of the quadrantid meteoroid stream. *MNRAS* 294, 127.
- Williams, I.P., Ryabova, G.O., Baturin, A.P., Chernitsov, A.M., 2004. The parent of the quadrantid meteoroid stream and asteroid 2003 EH1. *MNRAS* 355, 1171–1181.
- Williams, I.P., Wu, Z.D., 1993. The quadrantid meteoroid stream and comet 1491i. *MNRAS* 264, 659.
- Wisdom, J., Holman, M., 1991. Symplectic maps for the n -body problem. *Astron. J.* 102, 1528–1538.